Calibrating the late Smithian (Early Triassic) crisis: new insights from the Nanpanjiang Basin, South China.

Xu Dai, Zhiwei Yuan, Arnaud Brayard, Mingtao Li, Xiaokang Liu, Enhao Jia, Yong Du, Huyue Song, Haijun Song

Accepted version of:

Calibrating the late Smithian (Early Triassic) crisis: new insights from the Nanpanjiang Basin, South China

Published in: Global and Planetary Change, 2021, 201, 103492

Xu Dai[1], Zhiwei Yuan[1], Arnaud Brayard[2], Mingtao Li[3], Xiaokang Liu[1], Enhao Jia[1], Yong Du[1], Huyue Song[1], Haijun Song[1*]

[1]State Key Laboratory of Biogeology and Environmental Geology, School of Earth Sciences, China University of Geosciences, Wuhan 430074, China.

[2]Biogéosciences, UMR 6282, CNRS, Université Bourgogne Franche-Comté, 6 Boulevard Gabriel, 21000 Dijon, France.

[3]School of Geosciences, Yangtze University, Wuhan 430100, China

[*]Corresponding author, email: haijunsong@cug.edu.cn

ABSTRACT

The biotic recovery following the Permian/Triassic boundary mass extinction was influenced by several secondary extinctions during the Early Triassic, of which the late Smithian crisis is the most severe known for some nekto-pelagic organisms such as ammonoids. The Smithian-Spathian transition is characterized by successive global biotic and environmental changes, including a dramatic positive carbon isotopic excursion, oceanic anoxia and a cooling event beginning in the late Smithian. However, the tempo, modalities and the causal relationships among these various events remain poorly constrained. Here we synthesized paleontological, sedimentological, and geochemical data from three sections (Motianling, Nafang, and Shanggang) within the Nanpanjiang Basin, representing platform slop to basinal deposits spanning the Smithian/Spathian boundary. High-resolution analyses of thin sections show a sudden decrease in richness and abundance of fossil grains at the

middle/upper Smithian boundary in all three sections, coinciding with the onset of a positive shift in $\delta^{13}C_{carb}$. It also slightly precedes the beginning of the late Smithian cooling. At Shanggang, a change in dominance from bivalve-rich to ostracod-rich strata is also recorded at the middle/upper Smithian boundary. Overall, our results therefore indicate that a first major biotic crisis and turnover happened during the beginning of the late Smithian in the Nanpanjiang Basin, rather than around the Smithian/Spathian boundary. Complementary analyses on pyrite framboid size indicate that these observed biotic changes are concurrent with oxygen depletion in the studied sections, supporting the hypothesis that oceanic anoxia also played an important role in the late Smithian crisis in combination with climate cooling and oceanic acidification.

1. INTRODUCTION

After the largest known mass extinction at the Permian/Triassic boundary (PTB), the subsequent biotic recovery during the Early Triassic was a period characterized by recurrent deleterious environmental conditions (Song et al., 2012; Sun et al., 2012; Grasby et al., 2013a; Romano et al., 2013) and several secondary extinctions (Stanley, 2009; Jattiot et al., 2016; Foster et al., 2017), among which the late Smithian crisis (LSC, ~249.6 million years ago; Widmann et al., 2020) was probably the most severe. The LSC corresponds to climatic and marine environmental upheavals coeval to marked extinctions and turnovers in nekto-pelagic organisms such as ammonoids and conodonts (Orchard, 2007; Brayard et al., 2009; Goudemand et al., 2019; Song H.Y. et al., 2019). During this event, ammonoids suffered diversity and disparity bottlenecks, with e.g., the disappearance of ~80% of families and the transient loss of sphaeroconic forms (Brayard et al., 2009; Brühwiler et al., 2010a; Brosse et al., 2013; Zhang et al., 2019b). At the same time, ammonoids exhibit a marked change in paleogeographic distribution, becoming highly cosmopolitan (Brayard et al., 2006, 2007; Dai and Song, 2020). During the early late Smithian, ammonoid assemblages were dominated worldwide by iconic prionitids such as *Anasibirites* and *Wasatchites* (Tozer, 1981; Brayard et al., 2006; Brayard et al., 2007; Jattiot et al., 2016, 2018). Conodonts also show marked turnovers as well as size changes in segminate P1 elements during the late Smithian or near the Smithian/Spathian boundary (Orchard, 2007; Chen et al., 2013; Leu et al., 2019; Zhang et

al., 2019b). Overall, the LSC had a severe impact on nekton almost rivalling in intensity with that of the PTB mass extinction (Orchard, 2007; Brayard et al., 2009; Jattiot et al., 2016). However, this major event did not markedly delay the biotic recovery. For instance, ammonoids and conodonts show a remarkable diversification during the early Spathian (Orchard, 2007; Brayard et al., 2019). Benthos also shows a significant recovery in the Spathian (Song et al., 2011; Hofmann et al., 2014, 2015; Foster et al., 2017). In addition, a diverse and complex marine biota was recently documented from the earliest Spathian of the western USA basin (Brayard et al., 2017). Another key late Smithian change in the marine realm corresponds to the shift in taxonomic composition of marine predatory guilds, from fish/amphibian- to fish/reptile-dominated higher trophic levels (Scheyer et al., 2014).

From a geochemical point of view, this event corresponds to a marked, global, positive carbon isotope excursion beginning near the middle/upper Smithian boundary up to the lower Spathian, indicating large environmental perturbations during this interval (Payne et al., 2004; Tong et al., 2007; Song et al., 2013). Sun et al. (2012) initially postulated that lethally hot temperatures caused the LSC. However, new high-resolution oxygen isotope measurements from the Salt Range show a rapid climate cooling during the latest Smithian (Goudemand et al., 2019). Spore-pollen analyses show a rapid transition from the middle Smithian spore-dominated floras to the latest Smithian gymnosperm-dominated assemblages, reflecting a change from a humid, warm climate in the middle Smithian to a drier, cooler climate during the latest Smithian (Galfetti et al., 2007b; Hermann et al., 2012). This observation is also consistent with oxygen isotope trends. Apart from temperature changes, upper Smithian and Smithian/Spathian boundary dysoxic to anoxic deposits were often documented worldwide, including South China (Song et al., 2012; Sun et al., 2015; Song H.Y. et al., 2019), the Salt Range (Hermann et al., 2011), Arctic Canada (Grasby et al., 2013a), Iran (Zhang et al., 2018), Oman (Clarkson et al., 2016) and USA (Brayard et al., 2019). However, the exact timing, extent, and triggers of these anoxic deposits remain controversial (Clarkson et al., 2016; Song H.Y. et al., 2019; Zhang et al., 2019a). For instance, it has been hypothesized that the pre-late Smithian ocean potentially highly stagnated (Song et al., 2013) and that the late Smithian cooling restarted the global oceanic circulation and upwellings on continental margins, leading to transient local increases in marine productivity, expansion of

oceanic oxygen-minimum zones, and shelf acidification (Lyu et al., 2019; Song HY et al., 2019; Song et al., 2021). Another hypothesis is that the cooling event also generated a glacio-eustatic regression and consequently enhanced the deposit of anoxic sediments (Goudemand et al., 2019; Hammer et al., 2019).

Thus, the relationships between the LSC and coeval environmental and climate changes remain not completely constrained. Analyses of the biotic responses to the LSC are mainly derived from compilations of ammonoid and conodont diversity at a regional or global scale (Tozer, 1981; Orchard, 2007; Brayard et al., 2009; Brühwiler et al., 2010a; Zhang et al., 2019b). In this work, we synthesized paleontological, paleoredox and $\delta^{13}C$ analyses from three sections (Motianling, Shanggang, and Nafang) of the Nanpanjiang Basin, South China, to highlight the position of the first biotic changes corresponding to the LSC and to provide new insights on the potential relationships between the LSC and coeval environmental upheavals.

2. GEOLOGICAL BACKGROUND

2.1. Regional paleogeography and stratigraphy

The South China Block formed a stable paleogeographic element from the Late Proterozoic to the Late Triassic, mainly dominated by shallow-water carbonates during much of this time (Enos et al., 1998). Lower Triassic rocks are well exposed throughout South China (Yang et al., 1987; Tong et al., 2018). During the Early Triassic, the South China block was located at equatorial latitudes, at the interface between the Panthalassa and Tethys (Scotese, 2014). A large carbonate platform, the Yangtze Platform, was located in its center. The Nanpanjiang Basin embayed its southern margin. Several isolated carbonate platforms such as the Luodian Platform developed within the basin (Feng et al., 1997). Shallow-water limestones and dolostones dominate the Early Triassic deposits of the Yangtze Platform, whereas carbonates and siliciclastic series represented by the Luolou Formation dominate in the Nanpanjiang Basin. The lowermost deposits of the Luolou Formation include the iconic thick microbialite deposits of Griesbachian age, developed on carbonate platforms and representing the shallowest environments of the Luolou Formation (Galfetti et al., 2008;

Lehrmann et al., 2015; Bagherpour et al., 2017; Fang et al., 2017). The overlaying carbonate-siliciclastic unit is made of dark, thin-bedded, laminated mudstones alternating with organic-rich shales of Dienerian to Smithian age, suggesting oxygen-restricted and low-energy basin environments (Galfetti et al., 2008). Some sites on carbonate platforms were not influenced by massive siliciclastic inputs and showed a continuous carbonate succession, such as at the Motianling (Wu et al., 2019) and Nafang sections (this work). The carbonate-siliciclastic unit is overlain by massive nodular limestones of Spathian age, formed in well-oxygenated, medium- to high-energy environments (Galfetti et al., 2008).

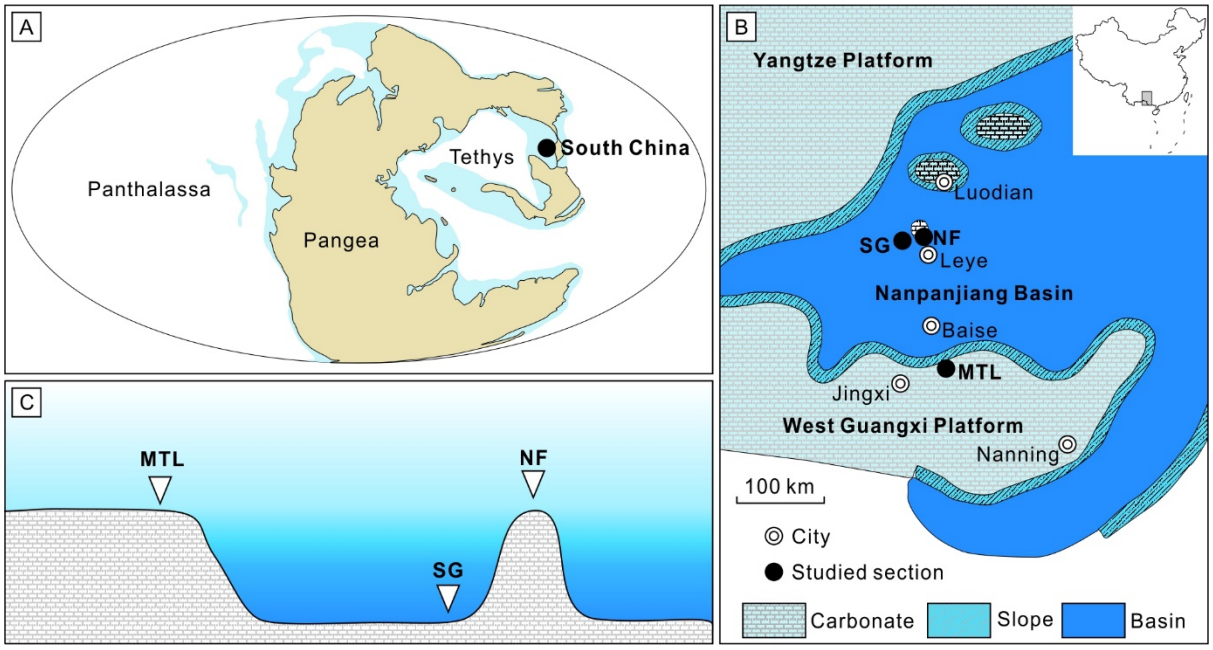

Figure 1. (A) Early Triassic paleogeographic map, modified from Scotese (2014). (B) Early Triassic paleogeographic map of the Nanpanjiang Basin, modified from Feng et al. (1997). (C) Schematic paleogeographic settings of the three studied sections. MTL—Motianling section; SG—Shanggang section; NF—Nafang section.

2.2. General Smithian biostratigraphy

The Early Triassic is officially divided into two stages, the Induan and Olenekian (Ogg, 2012). The latter is further subdivided into two substages, the Smithian and Spathian, based on ammonoid biostratigraphy (Tozer, 1965). This subdivision is widely used by the Early Triassic workers as the Smithian/Spathian boundary corresponds to the largest known intra-Early Triassic event (e.g., Brayard et al., 2009). However, the Smithian/Spathian

boundary has not been officially defined (e.g., Zhang et al., 2019). Based on ammonoids, it is commonly assumed that the Smithian/Spathian boundary can be placed between the late Smithian *Glyptophiceras*/*Xenoceltites* assemblage and the early Spathian *Bajarunia/Tirolites* assemblage (Brayard et al., 2019; Zhang et al., 2019b). Recently, Widmann et al. (2020) proposed a new latest Smithian ammonoid zone based on data from Nevada, western USA, which is younger than the *Glyptophiceras*/*Xenoceltites* assemblage. They therefore suggested that the Smithian/Spathian boundary should be placed within the separation interval between this new zone and the Tirolitidae n. gen. A zone. Zhao et al. (2007) claimed the use of the conodont *Novispathodus pingdingshanensis* as a marker for the Smithian/Spathian boundary. However, this proposal is still intensively debated (see e.g. discussion in Zhang et al., 2019a and Widmann et al., 2020). In this work, the biostratigraphic framework and the definition of the Smithian/Spathian boundary is mainly based on ammonoids, supplemented with recent conodont works conducted in the Nanpanjiang basin (Wu et al., 2019; Widmann et al., 2020).

The Smithian ammonoid biostratigraphy is presently the most well-constrained one among the four substages of the Early Triassic, benefiting from several recent extensive bed-by-bed fieldworks and detailed taxonomic revisions in the last decade (Brayard and Bucher, 2008; Shigeta et al., 2009, 2014; Brühwiler et al., 2010b, 2010c, 2011, 2012a, 2012b, 2012c; Brayard et al., 2013; Jattiot et al., 2016, 2017, 2020; Jenks and Brayard, 2018). Based on these works, the Smithian can be further subdivided into three parts: early, middle and late (Brühwiler et al., 2010a). These Smithian subdivisions can also be applied to the Nanpanjiang basin (Brayard and Bucher, 2008; Jenks et al., 2015).

2.3. Regional Smithian biostratigraphy

Chao (1959) conducted the first extensive study on Early Triassic ammonoids from the Nanpanjiang Basin. He established a preliminary zonation including eight ammonoid zones for the entire Early Triassic. In the last 15 years, Early Triassic ammonoid scales with a higher resolution were proposed for the Nanpanjiang Basin (Galfetti et al., 2007a; Mu et al., 2007; Brühwiler et al., 2008; Brayard and Bucher, 2008; Dai et al., 2019). Brayard and Bucher (2008) recognized four main ammonoid “beds” for the Smithian, i.e., *Kashmirites kapila* beds, *Flemingites rursiradiatus* beds, *Owenites koeneni* beds, and *Anasibirites*

169 *multiformis* beds, which can be further subdivided into successive horizons that can be
170 correlated worldwide (e.g., Jenks et al., 2015).
171 Early Triassic conodont biostratigraphy is still in progress for the Nanpanjiang Basin.
172 Although still debated, it often comprises more than ten zones for the entire Early Triassic
173 (Wu et al., 2019). Recently, eight conodont Unitary Association zones were proposed for the
174 early Smithian–early Spathian interval (Widmann et al., 2020). Some of these conodont zones
175 being only of regional significance with some uncertainty in long-distance correlation, we
176 consequently use the Smithian ammonoid biostratigraphic scale in this work.
177
178 **2.4. Studied sections**
179 The Motianling section (23°26’04"N, 106°57’17"E) was located in the northern
180 margin of the western Guangxi Platform during the Early Triassic (Fig. 1B, C). A late
181 Permian-Middle Triassic succession is well exposed at this site. The upper Permian Heshan
182 Formation is dominated by massive, gray, bioclastic limestones containing abundant
183 foraminifers, sponges, brachiopods and calcareous algae, representing a well-developed
184 shallow-water carbonate platform (Wu et al., 2019). The lower Triassic Luolou Formation is
185 composed of two main lithological units. The basal unit is made of microbialites. The
186 overlying unit is characterized by light gray, medium- to thick- bedded, argillaceous
187 limestones (Fig. 2A), with occasional occurrences of ash beds. This unit contains abundant
188 ammonoids (Fig. 2B). Wu et al. (2019) provided a comprehensive conodont biostratigraphical
189 scale for this section, including eleven conodont zones for the Luolou Formation. However,
190 only one conodont zone was recognized at this site for the entire Smithian.
191 The Nafang section (24°48’48"N, 106°32’56"E) is located about 3 km north of Leye
192 County (Fig. 1B). The lithological succession at Nafang is relatively similar to the Motianling
193 section (Fig. 2D). The base of the Luolou Formation is also characterized by microbial
194 deposits, overlain by massive, light gray limestones, which contain abundant ammonoids and
195 occasionally bivalve-rich beds (Fig. 2E). These calcareous deposits do not interfinger with
196 siliciclastic deposits. This suggests that the Nafang section was located on a rather isolated
197 highland within the Nanpanjiang Basin during the Early Triassic (Fig. 1C).
198 The Shanggang section (24°48’45"N, 106°32’32"E) is located 700 m west of the

Nafang section (Fig. 1B, C). The upper Permian Heshan Formation, lower Triassic Luolou Formation, and the middle Triassic Baifeng Formation are well exposed along a newly built road. The Heshan Formation is composed of massive, dark-gray bioclastic limestones showing centimetric to decametric irregular, dark chert concretions. The succession corresponding to the Luolou Formation is similar to the one already described by Galfetti et al. (2008) and Widman et al. (2020). The faunal content of the Griesbachian-Dienerian strata was documented in Brühwiler et al. (2008), Hautmann et al. (2010) and Kaim et al. (2010). The Smithian deposits are characterized by thin-bedded limestones alternating with dark shales. Part of their ammonoid content was preliminarily described by Brayard and Bucher (2008). The Spathian is mainly composed of massive nodular limestones (Fig. 2F), as thoroughly described in Galfetti et al. (2008). Widmann et al. (2020) provided a synthetic study of the Smithian-Spathian succession at Shanggang, including conodont biostratigraphy, U-Pb dating and carbon isotopes. These recent data thus provide a robust basis for stratigraphic correlation among studied sections.

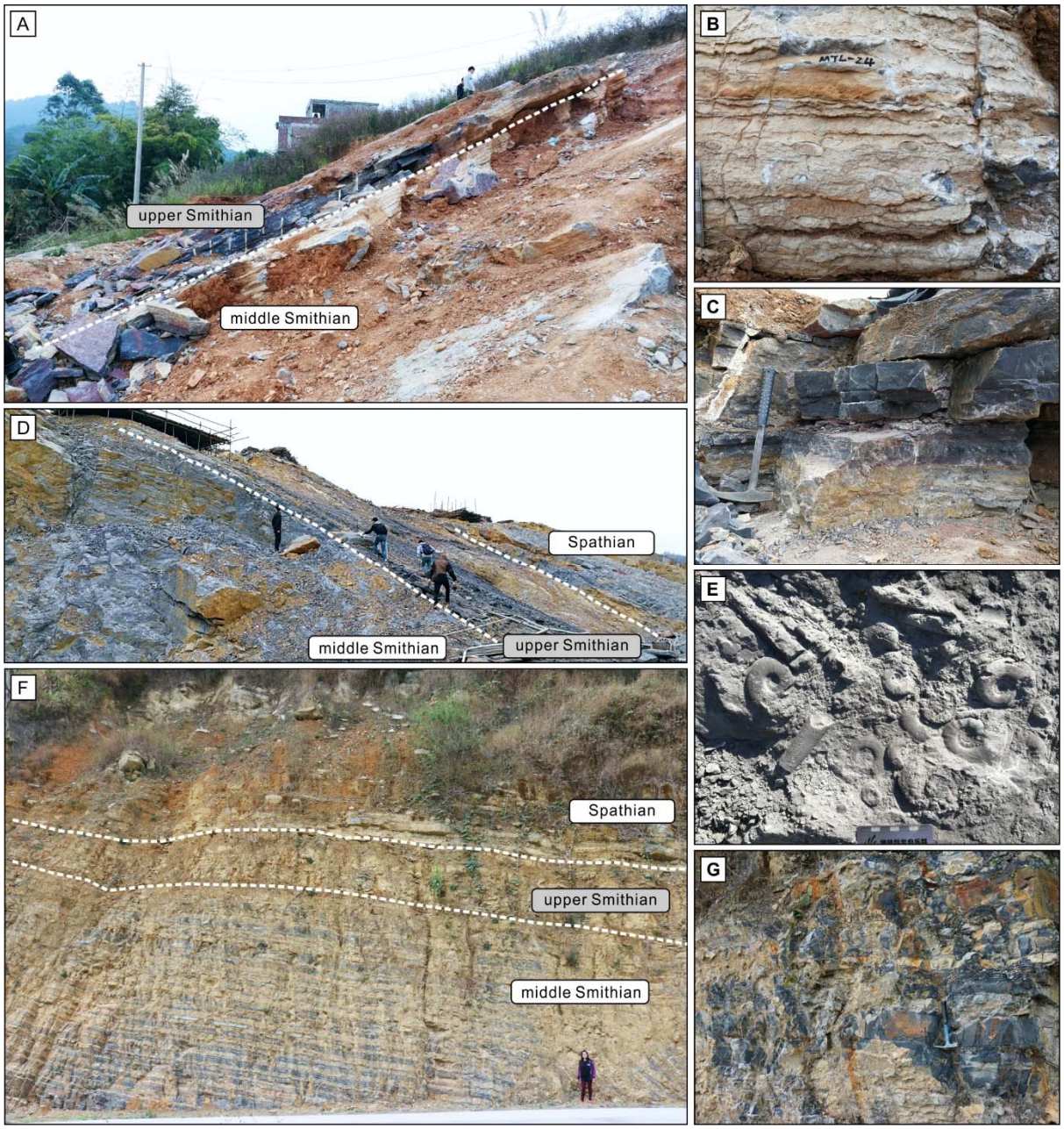

Figure 2. Field photos of the studied sites: (A) Motianling section, (B) bed MTL-24, containing abundant ammonoids at Motianling, (C) late Smithian strata at Motianling, showing dark limestones, (D) Nafang section, (E) abundant ammonoids from the *Xenoceltites variocostatus* Zone at Nafang, (F) Shanggang section, (G) black shales alternating with dark limestones and characterizing the late Smithian interval at Shanggang.

3. MATERIAL AND METHODS

3.1. Ammonoid study

Ammonoid specimens were collected bed-by-bed. However, some beds are highly cemented, preventing an easy excavation on the field. Careful preparation was performed using air tools to workout morphological details and thereby facilitate taxonomic assignment. Specimens were photographed using a Canon 70D camera with a Micro EF lens with 100 mm focal length and f/2.8 aperture. Taxonomic assignment mainly follows the classification proposed by Brayard and Bucher (2008) and refined by Jenks and Brayard (2018).

3.2. Carbon isotope analyses

Widmann et al. (2020) recently provided a high-resolution carbon isotope profile from Shanggang. We thus did not replicate similar analyses on Shanggang section. The Nafang succession is nearly identical to Motianling, both representing shallow-water settings. Thus, we only analyzed samples from the Motianling section. Thirty-eight limestone samples were collected from a ~5 m interval, covering the Smithian-Spathian transition, for carbon isotope analyses. Carbon isotopes were analyzed at the State Key Laboratory of Biogeology and Environmental Geology, China University of Geosciences, Wuhan. Powders were drilled using a dental drill after removing minor and weathered surfaces. About 300 μg powder was sealed into a 10 mL round-bottomed borosilicate vials, and reacted with 0.05 mL 99% orthophosphoric acid (Merck, Darmstadt, Germany, cat. #1.00565) at 72 °C after purged with 99.999% helium. The extracted CO_2 was then transported in a MAT253 isotope ratio mass spectrometer via a coupled Finnigan GasBench II interface to determine the carbon and oxygen isotope compositions. Isotopic values are reported as per mil notation (‰) with respect to the Vienna Pee Dee Belemnite (VPDB) standard, calibrated against laboratory standards GBW04416 ($\delta^{13}C$=1.61‰) and GBW04417 ($\delta^{13}C$=-6.06‰). The reproducibility of replicate analyses for standards and samples was better than ±0.1‰ for $\delta^{13}C$.

3.3. Thin section analyses and statistics of fossil grains

A total of 45, 39 and 46 thin sections were made for facies analysis and fossil grains statistics. Due to the highly cemented nature of the studied limestones, the extraction of macrofossils is often difficult, except in a few beds with abundant ammonoids. We therefore used grid counts of thin sections to quantitatively evaluate the abundance and richness of

fossil grains. This approach often sacrifices precise taxonomic identification, and thus, involves a taxonomic work only performed at a high rank, such as the order or the class. However thin section counts can quantitatively track the changes in abundance and richness of high taxonomic-level organisms. It can also be performed at a high stratigraphic resolution, which is often difficult for specimen-based taxonomic works. Additionally, the highly cemented nature of the rocks does not significantly bias this approach.

To carry out the grid count, we follow several steps. First, we set a standard 10×10 grid transparent slice with a single cell size of 1×1 mm. Then, we put this slice on a thin section and count the abundance of each kind of fossil grains under the microscope. We count 1 if they occur in a given cell and 0 if not. Finally, we sum their total number of occurrences within the one hundred cells. To avoid artificial count biases, the analyzed area was chosen randomly. We additionally choose two different areas to count twice in each thin section and calculate an average abundance for each identified group. The identification of biotic grains was performed with the help of the deep learning classifier of microfacies (www.ai-fossil.com, Liu and Song, 2020; website under construction).

3.4. Pyrite framboid analyses

Paleoredox conditions were tentatively reconstructed by pyrite framboid size analyses, following the approach of Bond and Wignall (2010) and Tian et al. (2014). These investigations complement sedimentological observations made on the field and thin section analyses. Fourteen and seventeen samples from the Motianling and Shanggang sections, respectively, were thus used to measure the size distribution of pyrite framboids potentially present in each sample. Samples were cut and polished at a size of ~2 × 2 cm. Pyrite framboid measurements were performed using a Zeiss reflection macroscope at the School of Earth Sciences, China University of Geosciences (Wuhan). A minimum of 100 pyrite framboids was measured for each sample when possible.

4. RESULTS

4.1. Ammonoid biostratigraphy

Based on bed-by-bed sampling and the previous work of Brayard and Bucher (2008) in Guangxi, we illustrate a high-resolution ammonoid framework for the three studied sections, spanning the middle to late Smithian and including four successive ammonoid zones. Two zones correspond to the middle Smithian: the *Flemingites rursiradiatus* and *Owenites koeneni* zones, and the other two are late Smithian: the *Anasibirites kingianus* and *Xenoceltites variocostatus* zones, in ascending order (Fig. 3). This succession is nearly identical to the one proposed by Brayard and Bucher (2008), except their initial *A. multiformis* beds, which are here further subdivided into two distinct zones, i.e., the lower *A. kingianus* Zone and the upper *X. variocostatus* Zone, which can be correlated worldwide (e.g., Jenks et al., 2015; Jattiot et al., 2017).

The *Flemingites rursiradiatus* Zone is defined on the occurrence of *F. rursiradiatus*. It contains a highly diversified ammonoid assemblage, including 24 genera (Chao, 1959, Brayard and Bucher, 2008). Common species are e.g., *Rohillites sobolevi*, *Submeekoceras mushbachanum*, *Pseudaspidites muthianus*, *Mesohedenstroemia kwangsiana* (Brayard and Bucher, 2008). At Shanggang, *F. rursiradiatus* was not found, but the occurrence of *Rohillites* sp. indet. and *S. mushbachanum* can be used for stratigraphic correlation, because the two genera are known so far only from the *F. rursiradiatus* zone in the Nanpanjiang Basin (Brayard and Bucher 2008). This zone corresponds to the lower *Novispathodus waageni* Zone at Motianling (Wu et al., 2019), and the conodont UAZ1 at Shanggang (Widmann et al., 2020).

The *Owenites koeneni* Zone is characterized by the occurrence of *O. koeneni*. This zone can be subdivided into three horizons, i.e., *Ussuria* horizon, *Hanielites* horizon and *Inyoites* horizon in ascending order (Brayard and Bucher, 2008). However, due to sporadic occurrence of these index genera in the studied sections, we are not able to use these detailed subdivisions. The *Owenites koeneni* Zone correlates well among sites from equatorial paleolatitudes and the North Indian Margin(e.g., Jenks et al., 2015). This ammonoid zone indicates a middle Smithian age and corresponds to the upper *Novispathodus waageni* Zone at Motianling (Wu et al., 2019), and the conodont UAZ2 at Shanggang (Widmann et al., 2020).

The *Anasibirites kingianus* Zone in the Nanpanjiang Basin contains the two genera

313 *Anasibirites* and *Hemiprionites* (Brayard and Bucher, 2008). This zone corresponds to the
314 conodont UAZ4 at Shanggang (Widmann et al., 2020) and indicates an early late Smithian
315 age. This low-diversity assemblage is represented by highly cosmopolitan ammonoid taxa
316 that can be used for worldwide correlation (e.g., Brayard et al., 2006, 2007; Jattiot et al.,
317 2018).

318 The *Xenoceltites variocostatus* Zone corresponds to the second zone of the late
319 Smithian and is characterized by the association of *X. variocostatus*, *Pseudosageceras*
320 *augustum*, and *Condensoceras youngi*. These taxa are also rather cosmopolitan and the *X.*
321 *variocostatus* Zone can therefore be correlated worldwide (Brayard and Bucher, 2008;
322 Shigeta et al., 2014; Jattiot et al., 2017; Jenks and Brayard, 2018). The *Xenoceltites*
323 *variocostatus* Zone correlates with the conodont UAZ5 at Shanggang (Widmann et al., 2020).
324 It can be noted that *Novispathodus pingdingshanensis* occurs in UAZ5, although this taxon
325 has been claimed as marker for the Smithian/Spathian boundary (see e.g. discussion in
326 Zhang et al., 2019 and Widmann et al., 2020). Its temporal distribution thus probably extends
327 from the late Smithian to early Spathian and it is thus probably better not to consider this
328 species as an appropriate marker for the Smithian/Spathian boundary. As this debate requires
329 more data and is beyond the scope of this work, we follow the original definition of the
330 Smithian and Spathian substage, proposed by Tozer (1965) based on ammonoid zones. Thus,
331 the *Xenoceltites variocostatus* Zone is considered to represent the latest Smithian in South
332 China.

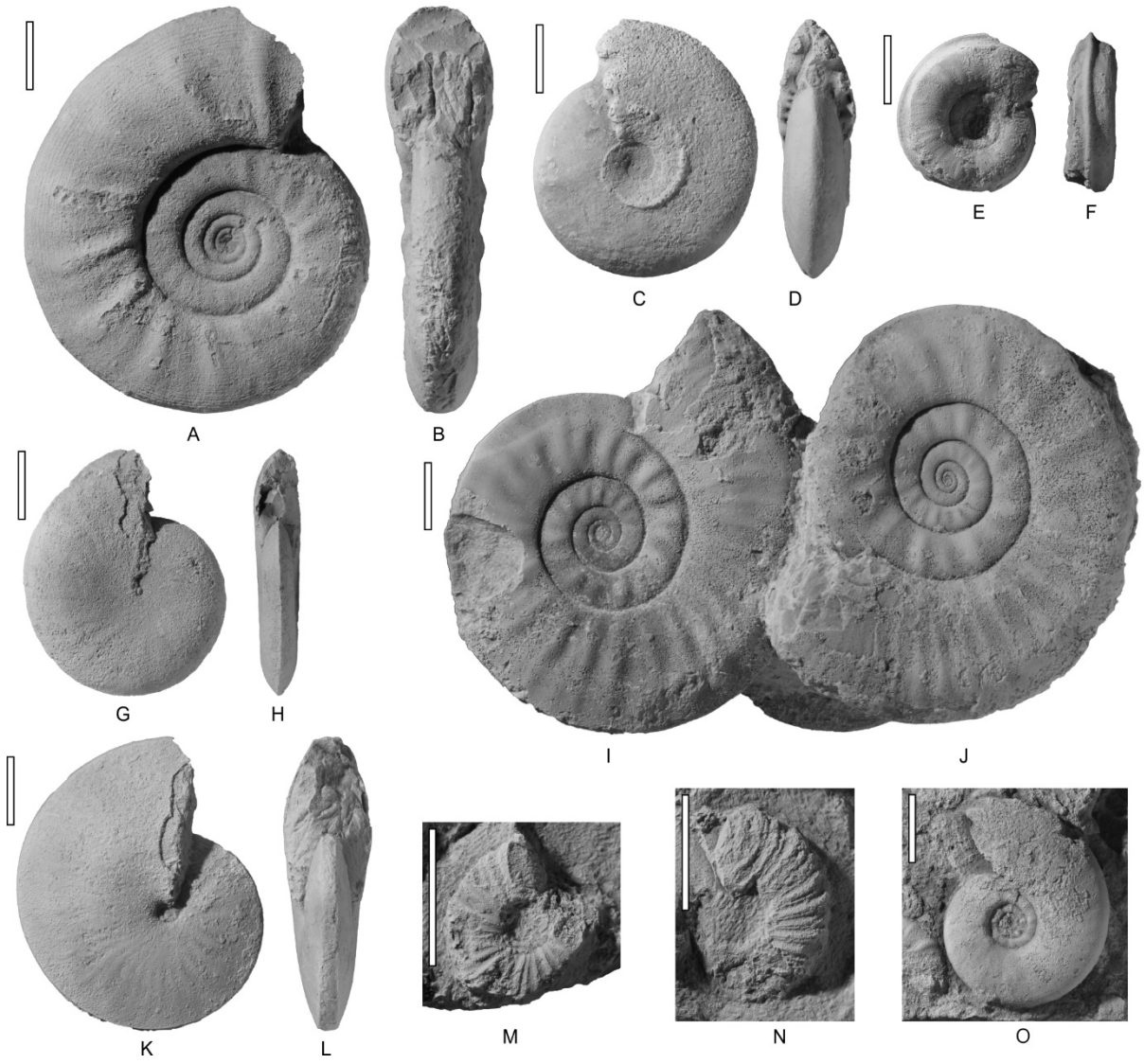

Figure 3. Typical middle and late Smithian ammonoids collected from the studied sections. (A, B) *Flemingites rursiradiatus*. (C, D) *Owenites koeneni*. (E, F). *Proharpoceras carinatitabulatum*. (G, H) *Aspenites acutus*. (I, J). *Rohillites sobolevi*. (K, L) *Mesohedenstroemia kwangsiana*. (M, N) *Anasibirites kingianus*. (O) *Xenoceltites variocostatus.* All specimens from Nafang section, except for M-N, from Motianling section. The scale bars represent 1 cm.

4.2. Facies analysis

The Smithian-Spathian successions of Motianling, Nafang, and Shanggang consist of seven facies that can be combined into three main facies associations, representing platform slope, deep shelf, and basin settings (Table 1, Fig. 4). Facies associations of the platform and deep shelf are prevalent in Motianling and Nafang, whilst deep basin settings occur only in

346 Shanggang.

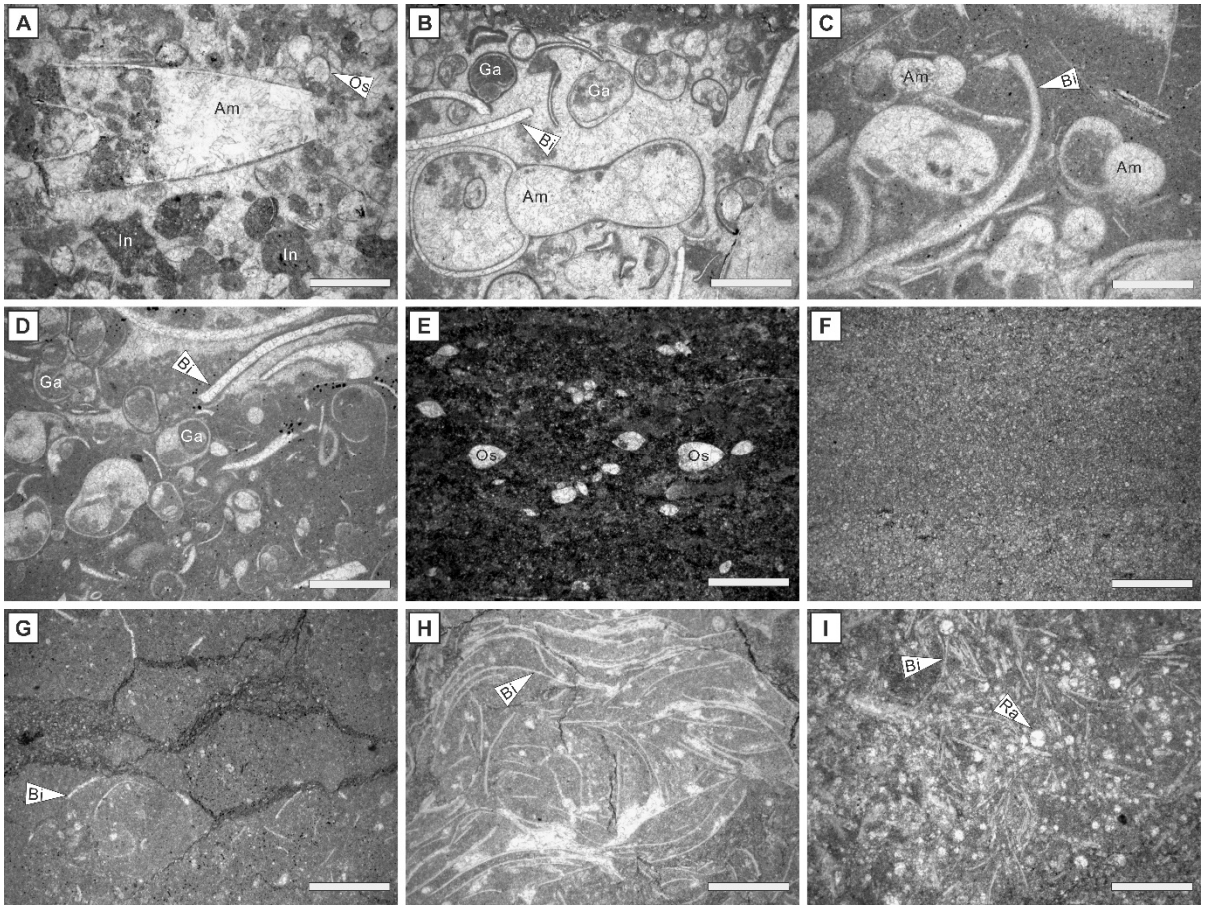

347

348 Figure 4. Photomicrographs of observed microfacies in the studied sections. (A)
349 Intraclast-rich grainstone (MF2); Motianling, Sample MTL-35b. (B) Gastropod-rich
350 grainstone (MF2); Motianling, Sample MTL-26b. (C) Bioclastic packstone with diverse
351 fossils (MF3). Nafang, Sample NF-139. (D) Bioclastic packstone with diverse fossils (MF3);
352 Motianling, Sample MTL-25b. (E) Bioclastic wackestone (MF4), the bioclasts are
353 represented by ostracods. Shanggang, Sample SG-144. (F) Lime mudstone (MF5);
354 Motianling, Sample MTL-30b. (G) Bioclastic wackestone showing nodular structure;
355 Motianling, Sample MTL-41. (H) Thin-shelled bivalve packstone; Shanggang, Sample
356 SG-157. (I) Calcispheres packstone with the occurrence of thin-shelled bivalves; Shanggang,
357 sample SG-125. Scale bar: 1 mm.

358

359 **4.2.1. Motianling section**

360 **Description**: The middle Smithian interval in Motianling comprises greyish-banded
361 limestone and yellowish marlstone. Banded limestone mainly consists of gastropod-rich

grainstone (MF1, Fig. 4B), bioclastic packstone (MF3), and nodular bioclastic wackestone (MF4). The upper Smithian succession consists of dark grey limestone and is characterized by its macrofossil paucity. Bioclasts are rare in the dark grey limestones excepting two levels that consist of intraclast grainstone (MF2) in which ostracods are abundant. The overlying lower Spathian succession is composed of nodular limestone that is mainly represented by low energy facies, including bioclastic wackestone (MF4) and lime mudstone (MF5) (Fig. 5).

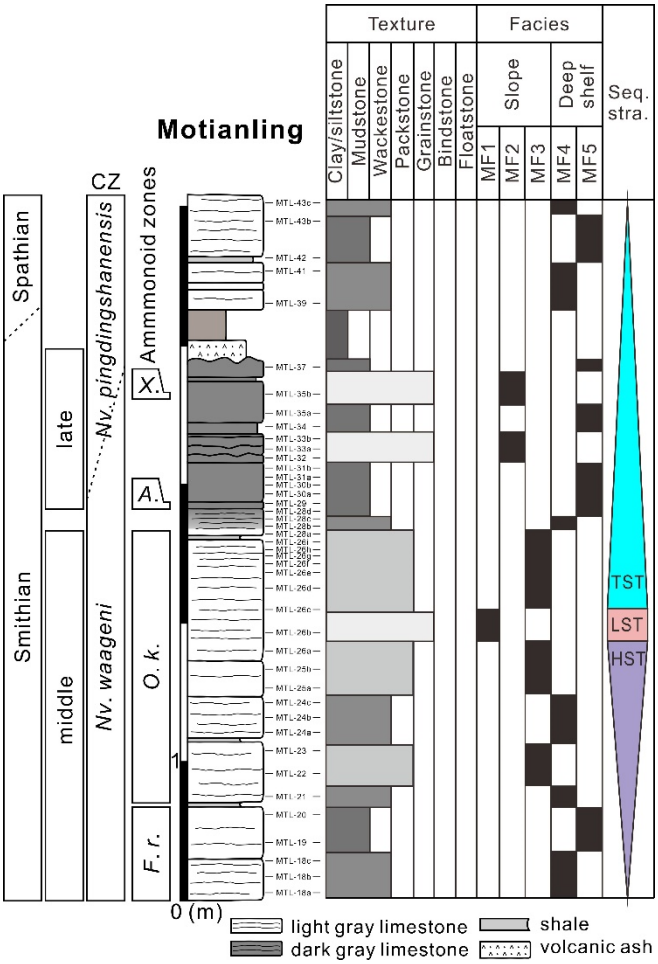

Figure 5. Sequence stratigraphy and microfacies evolution from the middle Smithian to the lower Spathian at Motianling. Abbreviations: CZ—conodont zones. *Nv.*—*Novispathodus*. *X.*—*Xenoceltites variocostatus*. *A.*—*Anasibirites kingianus*. *O. k.*—*Owenites koeneni*. *F. r.*—*Flemingites rursiradiatus*. Seq. stra.—Sequence stratigraphy. TST—transgressive systems tract. LST—lowstand systems tract. HST—highland systems tract.

374 Table 1. Microfacies classification and description. The standard microfacies refer to Flügel (2010).

Microfacies	**Biogenic content and texture**	**Sedimentary structure**	**Standard microfacies**	**Depositional setting**
MF1 Gastropod-rich grainstone	Abundant gastropods, common bivalves and ammonoids; Poorly sorted bioclasts cemented by sparry calcite.	Banded limestone intercalated with marls.	SMF 5	Platform slope
MF2 Intraclast grainstone	Abundant intraclasts with occasional ostracods; Moderately sorted bioclasts with sparry calcite.	Ripple laminated limestone	SMF 4	
MF3 Bioclastic packstone with diverse fossils	Common gastropods and bivalves, occasional ammonoids; Geopetal structures developed in shells of gastropods and ammonoids.	Massive limestone with thin banded marl intercalations.	SMF 5	
MF4 Ostracod wackestone	Occasional ostracods with rare thin-shelled bivalves.	Thin, fine laminated limestone	SMF 10	Deep shelf
MF5 Lime mudstone	Rare ostracods, thin-shelled bivalves.	Massive limestone	SMF 3	
MF6 Thin-shelled bivalve packstone	Abundant thin-shelled bivalves and rare ostracods or calcispheres.	Thin bedded limestone	SMF 12	Basin
MF7 Calcispheres-rich packstone/wackestone	Abundant calcispheres and common thin-shelled bivalves.	Horizontally laminated limestone	SMF 3	

Interpretation: The vertical distribution of Smithian-Spathian microfacies in Motianling shows a gradual deepening-upward trend, a transition from carbonate platform slope to deep shelf. The Smithian sequence is characterized by the occurrence of gastropod-rich grainstone (MF1) and mollusk-dominated packstone (MF3). Allochthonous bioclasts (i.e., gastropods, bivalves, and ammonoids) in MF1 are poorly sorted and highly abraded, and show a fining-upward trend, as well as a sharp lower erosive boundary, suggesting they correspond to tempestite deposits (Flügel, 2010; Pérez-López and Pérez-Valera, 2012). The randomly oriented geopetal fabrics in the shells of MF3, indicate reworking and redeposition, supporting a middle Smithian sequence deposited in high-hydrodynamic settings of the platform slope to deep shelf. The upper Smithian interval mainly consists of nodular wackestone/lime mudstone (MF5). Two thin layers of intraclast-rich grainstone (MF2) are interbedded with MF5. The MF2 intraclasts are poorly rounded and weakly sorted, indicating they were probably formed near or in the storm wave base on the platform slope and rapidly transported into the deep shelf.

4.2.2. Nafang section

Description: The middle Smithian succession in Nafang is mainly composed of massive limestones. Yellowish marlstones are absent. This differs from the Motianling succession. The massive limestone is rich in bioclasts including ammonoids and gastropods, which constitute the main component of bioclastic packstone (MF3). The upper Smithian interval is composed of dark grey limestone lacking macro- and micro-fossils, excepting one thin layer in which ostracods are abundant. The overlying lower Spathian interval is composed of thin-bedded bioclastic wackestone (MF4) (Fig. 6).

Interpretation: The middle Smithian succession corresponds to packstone-dominated limestones in which abundant macrofossils (especially gastropods and ammonoids) are well preserved. Geopetal fabrics are common but are oriented randomly, suggesting a reworking of shells after deposition by distal storm waves (Kidwell, 1991; Chatalov, 2013). The upper Smithian sequence is dominated by lime mudstones with very rare occurrences of fossils. A thin layer with abundant ostracods intercalated in the lime mudstones, similar ostracods rich beds also documented at Waili Fall section (Galfetti et al., 2008). The lower Spathian succession consists of monotonous bioclastic wackestones, indicating a stable deeper shelf setting. Overall, the Smithian-Spathian sequence shows a deepening-upward trend, similar to that of Motianling.

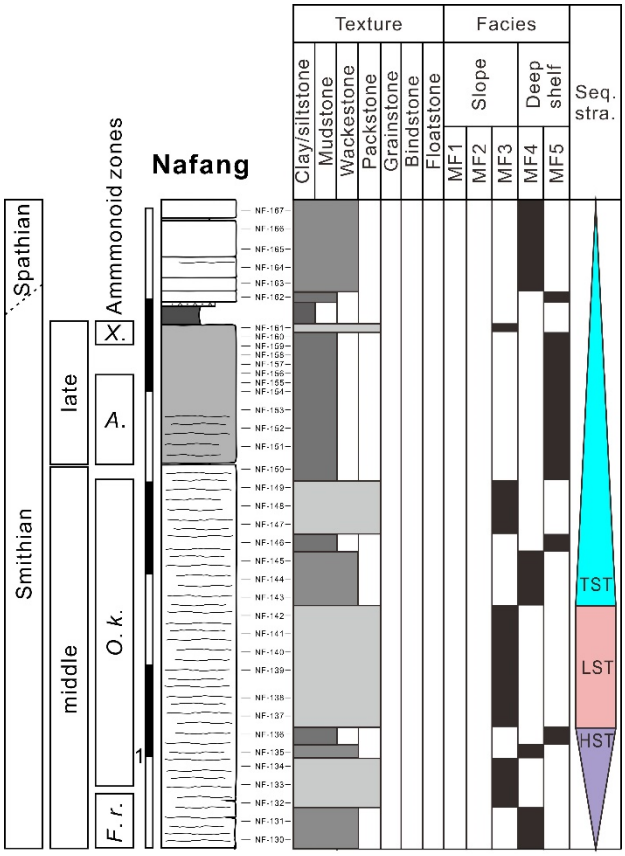

Figure 6. Sequence stratigraphy and microfacies evolution from the middle Smithian to the lower Spathian at Nafang. Abbreviations: see Figure 5.

4.2.3. Shanggang section

Description: The middle Smithian succession is composed of planar laminated, greenish mudstone intercalated with thin layers of limestone in which bioclasts are represented by thin-shelled bivalves (MF6) and calcified calcispheres (MF7). The upper Smithian interval consists of dark grey limestones embedded in black shales. The upper Smithian biofacies are comparable with their counterparts in Motianling and Nafang, all of which are characterized by their organic-rich levels and the concentration of ostracods in thin layers of dark grey limestones. The overlying lower Spathian succession is dominated by nodular/ribbon limestone consisted of densely packed thin-shelled bivalves (MF6) (Fig. 7).

Interpretation: The Smithian and Spathian successions of the shanggang section is identical to the section from the Jinya/Waili area, mainly dominated by basinal facies (Galfetti et al., 2008). Facies of the middle Smithian interval are interpreted as basinal deep-water facies (Galfetti et al., 2008; Flügel, 2010; Li et al., 2019). It is noteworthy that the middle Smithian lithofacies are highly similar to coeval deposits in the deep-water section of Xiukang, South Tibet (Li et al., 2019). The Smithian-Spathian sequence only contains two system tracts with

the lack of lowstand system tract, a pattern that is different from that of Motianling and Nafang. This is probably because that Shanggang was deposited in deeper settings, which were less influenced by relative sea level fluctuations.

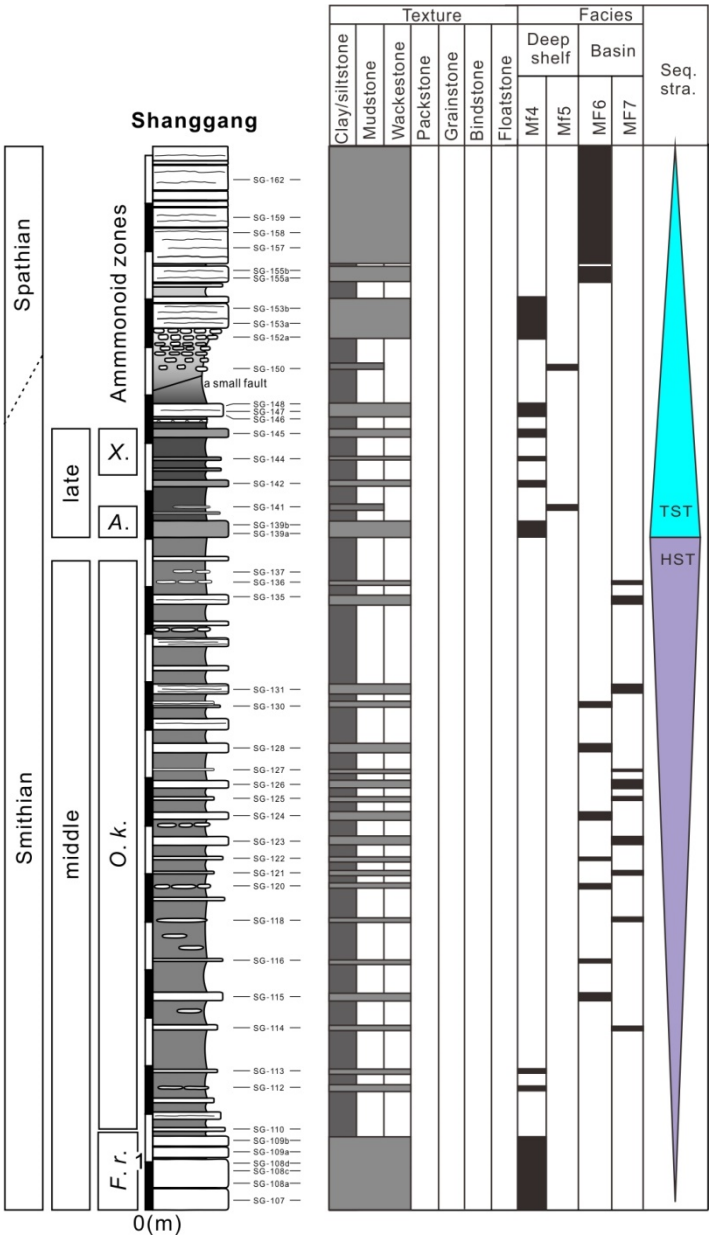

Figure 7. Sequence stratigraphy and microfacies evolution from the middle Smithian to the lower Spathian at Shanggang. Abbreviations: see Figure 5.

4.3. Carbon isotope profile

The carbon isotope signal obtained from the Motianling section displays an overall variation from -3.5‰ to 2.8‰ during the middle Smithian to the earliest Spathian (Fig. 8). It shows a gradual decrease across the *Flemingites rursiradiatus* Zone, followed by a slightly

positive shift at the top of this zone, and then, a plateau around 1‰ in the lower *Owenites koeneni* Zone. A second drop is observed in the middle of the *O. koeneni* Zone, followed by a fluctuating signal ranging from -3.5‰ to 0.5‰. A positive excursion is recorded from the base of the late Smithian up to the early Spathian. This positive shift is also documented at Shanggang (Widmann et al., 2020, their fig. 6), in neighboring sections (e.g., Galfetti et al., 2007) and worldwide (e.g., Zhang et al., 2019).

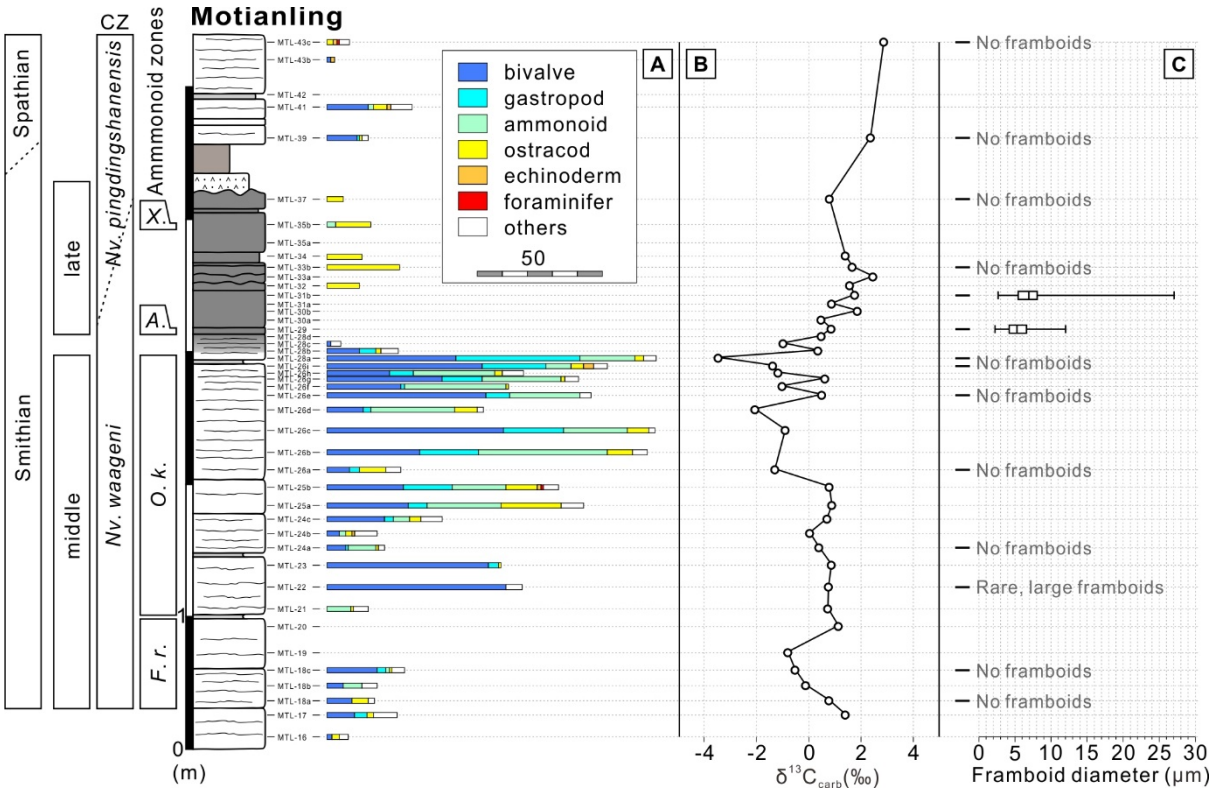

Figure 8. Paleontological and environmental analyses from the Motianling section. (A) Count of fossil grains: the bars represent the number of grid cells containing each kind of grains per one hundred cells. (B) Carbon isotope curve. (C) Pyrite framboid size measurements. Abbreviations: see Figure 5.

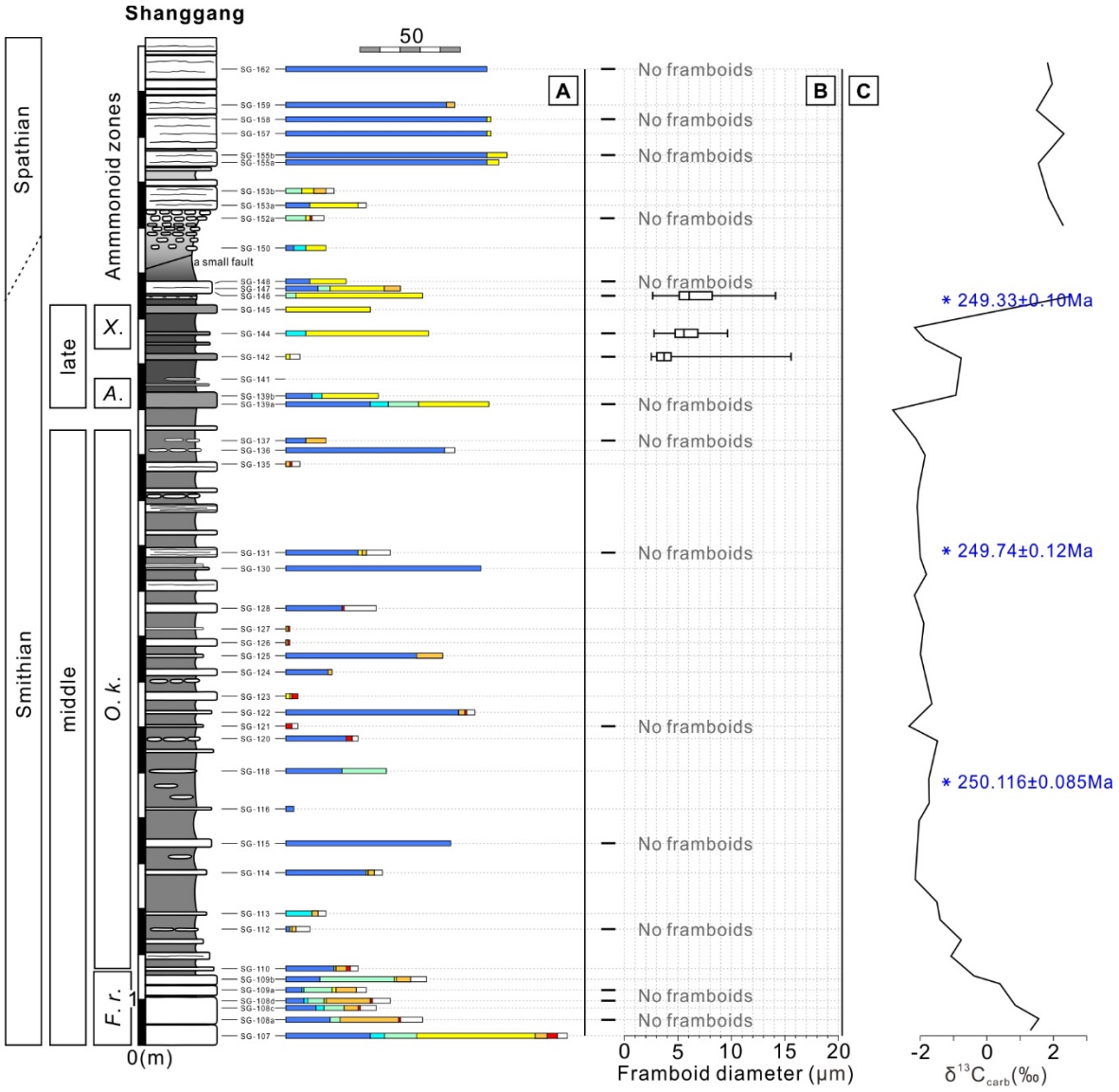

Figure 9. Paleontological and environmental analyses from the Shanggang section. (A) Fossil grains. (B) Pyrite framboid measurements. (C) Carbon isotope curve and U-Pb ages, modified from Widmann et al. (2020). Abbreviations: see Figure 5.

4.4. Fossil grains

Overall, the middle Smithian strata mainly contain mollusk remains (i.e., bivalves, ammonoids, and gastropods), whereas overlying late Smithian deposits are dominated by ostracods in all studied sections (Figs. 8-10).

At Motianling and Nafang, strata corresponding to the *Flemingites rursiradiatus* and *Owenites koeneni* Zones include abundant and diverse grains, dominated by mollusks (e.g., bivalves and ammonoids). At the middle/upper Smithian boundary, fossil grains show a dramatic decrease in diversity and abundance. The late Smithian is here exclusively characterized by occasional occurrences of ostracod grains. In the early Spathian, the

diversity and abundance of grains show a weak increase.

At Shanggang, fossil grains are abundant and diverse in the *Flemingites rursiradiatus* Zone. The *Owenites koeneni* Zone is exclusively dominated by bivalves. At the middle/upper Smithian boundary, fossil grains show a shift in dominance, from bivalves to ostracods. Across the Smithian/Spathian boundary, the abundance in ostracod grains decreased, followed by an abrupt increase of bivalve particles during the early Spathian.

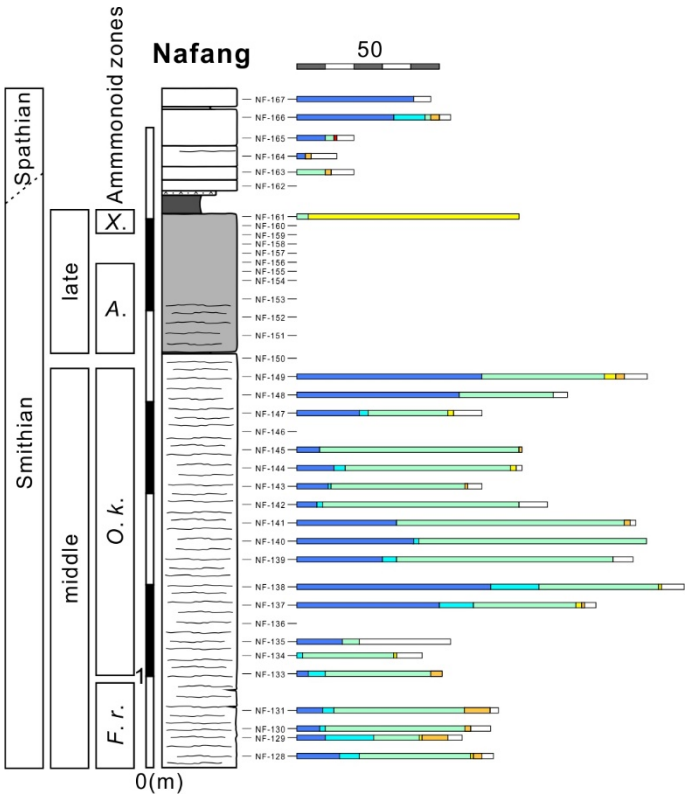

Figure 10. Temporal evolution of fossil grains at Nafang section. for Abbreviations: see Figure 5.

4.5. Paleoredox conditions

The reconstruction of paleoredox history is based on microfacies and pyrite framboid analyses. 14 and 17 samples from Motianling and Shanggang were polished for pyrite framboid analyses, respectively. Two samples from Motianling and three samples from Shanggang yield abundant pyrite framboids (Figs. 8, 9). Other samples contain a few large or no pyrite framboids.

At Motianling, the middle Smithian samples do not contain pyrite framboids. This interval is characterized by bioclastic packstones with abundant ammonoids and a few gastropods, corresponding to well-oxygenated slope facies (Figs. 2B, 5). Two (MTL-29 and MTL-31) of the four samples from the late Smithian show abundant framboids. The late

Smithian strata are made of dark finely-laminated mudstone intercalated with ostracod-rich grainstone, suggesting dysoxic to anoxic deep shelf settings (Figs. 2C, 5). The two samples from the early Spathian do not show any pyrite framboids. MTL-29 contains small framboids (mean diameter = 5.46 μm; Fig. 11A) with a small standard deviation (1.77), suggesting potential euxinic-anoxic conditions (Fig. 11F), based on the method of Bond and Wignall (2010) and Tian et al. (2014). Framboids in sample MTL-31 have a larger mean diameter (7.08 μm; Fig. 11B) and standard deviation (2.91), suggesting a dysoxic environment (Fig. 11F). Pyrite framboids data are thus consistent with sedimentary observations.

At the Shanggang section, middle Smithian samples do not contain pyrite framboids. However, the middle Smithian interval at Shanggang is dominated by dark shales interbedded with thin limestones, likely corresponding to oxygen-poor deep shelf settings. Two (SG-142 and SG-144) of the three samples from the late Smithian exhibit abundant framboids. The late Smithian interval is dominated by black shales and black finely-laminated ostracod-rich wackestones (Figs. 2G, 4E, 7), suggesting a deep shelf oxygen-poor environment, identical to the upper Unit IV described from the Luolou Formation by Galfetti et al. (2008). In the six remaining samples, only one near the Smithian/Spathian boundary contains pyrite framboids. Framboids from samples SG-142 and SG-144 exhibit small mean diameters (4.01 μm and 5.82 μm, respectively; Figs. 11C, D) with small standard deviations (1.78, and 1.60, respectively). These values suggest potential euxinic-anoxic conditions for the corresponding beds (Fig. 11F). SG-146 contains large pyrite framboids (mean diameter = 6.60 μm; Figs. 11E) with a large standard deviation (2.22), indicating a potential dysoxic environment (Fig. 11F).

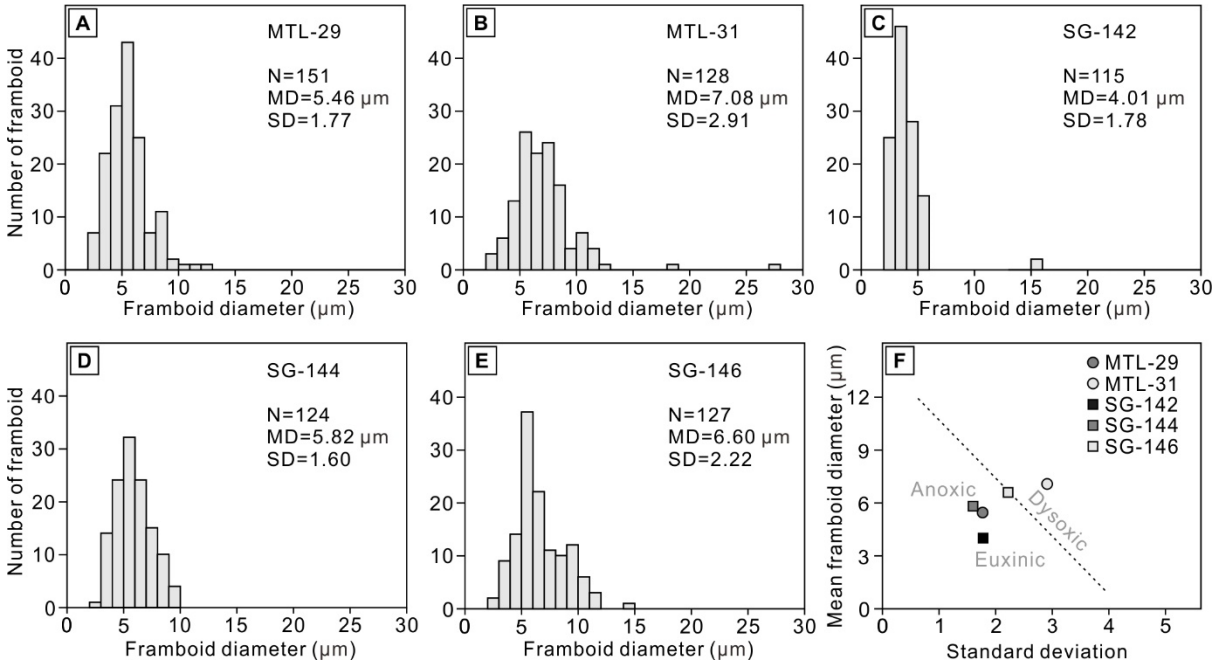

Figure 11. Size distributions of pyrite framboids in late Smithian strata of Motianling and Shanggang (A-E) and corresponding interpreted redox conditions (F). MTL—Motianling; SG—Shanggang.

5. DISCUSSION

5.1. Timing and modalities of the late Smithian crisis

The successive global events occurring near the Smithian/Spathian boundary were often previously referred to as the "Smithian/Spathian boundary extinction" (Galfetti et al., 2007b; Stanley, 2009; Sun et al., 2012; Chen et al., 2013; Sun et al., 2015; Grasby et al., 2016). However, recent progresses in biostratigraphy showed that the first dramatic diversity drop associated with changes in the spatial distribution of taxa is actually at the middle/upper Smithian boundary, at least for some nekto-pelagic taxa (Orchard, 2007; Brayard et al., 2009; Brühwiler et al., 2010a).

The LSC has an almost equal impact on ammonoids as the PTB mass extinction (Brayard et al., 2009; Jattiot et al., 2016) eliminating ~75% ammonoid families (Zhang et al., 2019b), coinciding with a severe disparity decrease (Brosse et al., 2013) and a marked cosmopolitanism episode (Tozer, 1981; Brayard et al., 2006; Brayard et al., 2007; Jattiot et al., 2018). Conodonts also exhibit a diversity bottleneck during this time interval (Orchard, 2007). In addition, it corresponds to a size reduction in segminate P1 elements, and a gradual increase in segminiplanate P1 elements (Chen et al., 2013; Leu et al., 2019). Apart from the

nekton crisis, data from western USA, Dolomites, Hungary, and Lombardy suggest that benthic ecosystems apparently do not show any remarkable changes during the late Smithian and the Smithian/Spathian transition, but a potential faunal turnover in the early Spathian (Hofmann et al., 2014, 2015; Foster et al., 2015, 2017, 2018). Foraminifer data from South China show a temporary pause in their diversification, but no marked extinctions or turnovers during the late Smithian (Song et al., 2011). Therefore, based on presently known data, the LSC has maybe only a few impacts on benthic ecosystems. Intrinsic factors (e.g., evolutionary rates) or interspecific competition might be a plausible explanation of this discrepancy between benthic and nekto-pelagic organisms during the late Smithian (e.g., Stanley, 2009; Hautmann et al., 2015). However, it should be noticed that the exact content of Early Triassic benthic ecosystems at that time is far to be well constrained (e.g., Brayard et al., 2017).

At Motianling (shallow-water environment), fossil grains are abundant and diverse during the middle Smithian (Fig. 8). This echoes the known concomitant remarkable diversification of e.g., ammonoids, conodonts, and foraminifers (Orchard, 2007; Brayard et al., 2009; Song et al., 2011). At Shanggang (deeper water settings), fossil grains show a clade-diversity loss between the *Flemingites rursiradiatus* and *Owenites koeneni* Zones (Fig. 9). This decrease may result from facies change, corresponding to a transition from deep shelf to basin environment (Fig. 7).

A major turnover is visible at the boundary between the *Owenites koeneni* and *Anasibirites kingianus* Zones, i.e., at the middle/upper Smithian boundary, in the three studied sections. This turnover is not a result of a sedimentary facies change, as there are no significant facies change at Motianling and Shanggang. This boundary also coincides with the onset of the positive carbon isotopic excursion and disoxic/anoxic conditions (Fig. 12).

At Motianling and Nafang, the base of the late Smithian corresponds to a severe decrease in the abundance and diversity of fossil particles (Fig. 8, 10). The same time interval corresponds to a turnover from mollusk-dominated facies to ostracod-dominated facies in the deeper water settings of Shanggang. Ostracods notably show a bloom in both shallow and deep-water environments during the late Smithian. One potential explanation is that ostracods which often show a high tolerance to temperature changes and anoxia in modern contexts (Song et al., 2014), can have better survived to marked environmental fluctuations known for the LSC. Similar ostracod blooms are also reported from various Early Triassic exposures (Forel et al., 2013; Wan et al., 2019; Gliwa et al., 2020).

Our data suggest a potential heterogeneous impact of the LSC on benthic ecosystems

depending on their environmental settings. Hence, further studies at different paleogeographic locations and in various paleoenvironments at a larger spatial scale are a prerequisite to elucidate these differential effects.

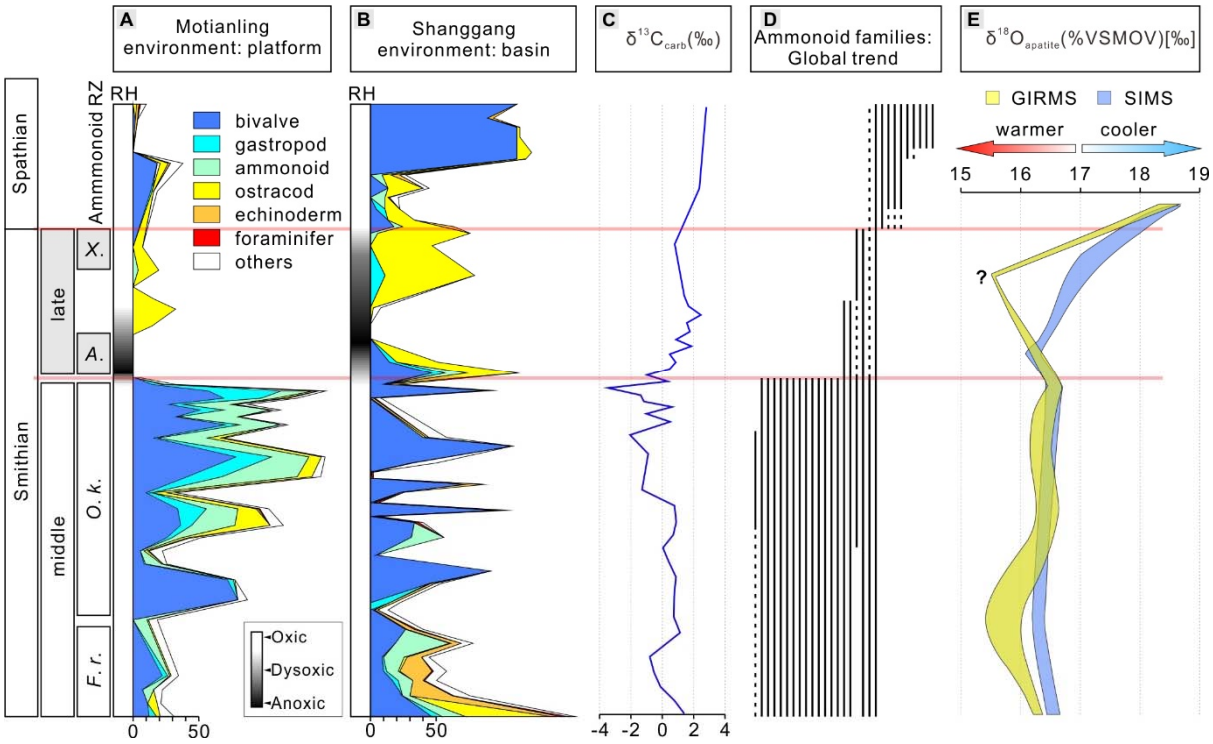

Figure 12. Simplified trends of local fossil grain count, global ammonoid family richness and environmental proxies around the late Smithian. (A) Count of fossil grains at Motianling. (B) Count of fossil grains at Shanggang. (C) Carbon isotope curve from Motianling section. (D) Global ammonoid family trend, modified from Zhang et al. (2019b). (E) Oxygen isotope curves, modified from Goudemand et al. (2019). RH—redox history. Abbreviations: see Figure 5.

5.2. Insights on environmental triggers of the late Smithian events.

A series of environmental upheavals were documented around the middle/upper Smithian boundary, mainly including: (i) a warm episode during the middle Smithian followed by a cooling event during the late Smithian (Goudemand et al., 2019), (ii) the occurrence of dysoxic to anoxic deposits in several basins (Grasby et al., 2013a; Song et al., 2014; Song H.Y. et al., 2019), and more recently (iii) Hg poisoning (Grasby et al., 2016). These changes were assumed to have triggered the LSC or to have been a consequence of this event (e.g., Grasby et al., 2013a; Goudemand et al., 2019). Causal relationships among these different parameters therefore remain partly unclear.

5.2.1. Oceanic anoxia and acidification

The studied sections show an anoxic/dysoxic event in both shallow- and deep-water settings during the late Smithian (Fig. 12A, B). The onset of this anoxic event in shallow-water settings is coeval with the reduction of fossil grains, suggesting a causal relationship.

Anoxia is a potential killing mechanism in many past extinctions, e.g., at the PTB (Wignall and Twitchett, 1996) and during the Toarcian (Bailey et al., 2003). Late Smithian-earliest Spathian anoxic deposits were also documented in e.g., Salt Range (Hermann et al., 2011), North Vietnam (Komatsu et al., 2016), Arctic Canada (Grasby et al., 2013a), South China (Song et al., 2012; Sun et al., 2015; Song H.Y. et al., 2019; Zhao et al., 2020). Recent calcium isotope analyses suggested a shelf acidification event associated with the anoxia event during the late Smithian-earliest Spathian interval (Song et al., 2021). This widespread anoxia as well as potential acidification thus could have contributed to the LSC. In this hypothesis, benthic organisms should have been more vulnerable than nekto-pelagic organisms, who can supposedly benefit from their higher mobility (Bambach et al., 2002; Song et al., 2018). However, ammonoids and conodonts show a marked extinction (Orchard, 2007; Brayard et al., 2009; Hofmann et al., 2014; Hofmann et al., 2015). In addition, no evidence for anoxia was found at some places and on isolated highs (e.g., Clarkson et al., 2016), although ammonoids also exhibit here a diversity drop like in any other locations (Brühwiler et al., 2012a). This thus suggests that anoxia and acidification probably contributed to the LSC but were likely not the main driver of nektonic taxa extinction.

5.2.2. Temperature change

Changes in sea surface temperature (SST) is commonly suggested to be one of the main triggers of the late Smithian events. Sun et al. (2012) initially reported a thermal maximum at the Smithian/Spathian boundary. However, after revision of used biostratigraphical markers and new sensitive high-resolution ion microprobe analyses, this thermal maximum is now suggested to occur near the middle/upper Smithian boundary or at the beginning of the early late Smithian (Goudemand et al., 2013, 2019; Zhang et al., 2019b). The late Smithian thus mainly corresponds to a marked SST decrease event from this thermal maximum. The LSC nekton diversity drop is consequently associated with complex SST changes, and notably with a marked decrease, preventing a simple causal relationship between high-SST and biotic extinction, as initially proposed by Sun et al. (2012).

The evolutionary rates of ammonoids and conodonts were very high during the

Smithian (Orchard, 2007; Stanley, 2009; Brühwiler et al., 2010a). These high intrinsic evolutionary rates can have helped to some extent these organisms to display rapid rediversification during the Early Triassic (Stanley, 2009). Based on data from Pakistan, the late Smithian cooling mainly occurred from the *Wasatchites distractus* Zone to the earliest Spathian (Goudemand et al., 2019). This short time interval (~500 kyr; Widmann et al., 2020) with such relatively rapid SST decrease after a marked warm climate during the middle Smithian, may have been beyond the physiological tolerances of most ammonoids and conodonts. So, the rate of the SST change is potentially as crucial as its magnitude to lead to biotic extinction (Mathes et al., 2021).

5.2.3. Hg poisoning

Mercury anomalies are usually associated with releases of large igneous provinces. They were thus used as a putative signal of volcanic activities during the geological past (Thibodeau et al., 2016; Charbonnier and Follmi, 2017; Grasby et al., 2017; Wang et al., 2018). Hg poisoning generated by volcanism was recently proposed to be an additional killing mechanism participating in the LSC (Grasby et al., 2016). These authors documented Hg enrichments, assumed to be toxic to the ecosystem, during the early late Smithian in shallow-water settings from western Spitsbergen. However, Hammer et al. (2019) reported Hg anomalies mainly occurring within the middle Smithian of central Spitsbergen. This casts doubt on a direct link between Hg anomalies and the late Smithian crisis. Additionally, Hg contents in Chaohu (South China), Guryul Ravine (Kashmir), and Arctic Canada do not show any remarkable increase during the late Smithian (Grasby et al., 2013b; Wang et al., 2019). To sum up, only a few sections recorded so far mercury anomalies during the late Smithian, suggesting that volcanism poisoning, if real, had only a very limited geographic impact (Wang et al., 2019). Overall, there is no direct evidence supporting a causal relationship of Hg anomaly to the late Smithian crisis.

In summary, global temperature fluctuations secondarily associated with oceanic anoxia most likely caused the LSC (Song et al., 2014). Volcanic activities were probably only responsible for some local to regional stresses (Wang et al., 2019). Further studies combining primary productivity, eustatic fluctuations, with high-resolution biostratigraphic constraints could be helpful to fully decipher the primary causes of the LSC.

5.3. Recovery from the LSC

The LSC corresponds to a relatively short interval spanning the two ammonoid zones

of the late Smithian in the Nanpanjiang Basin (Fig. 12). Above the Smithian/Spathian boundary, fossil grains show a small rebound in diversity and abundance in both shallow and deeper water settings (Figs. 8-10). This increase does not result from sedimentary facies shift (Figs. 5-7). This therefore probably suggests a rather rapid restoration of regional communities after the LSC. Ammonoids and conodonts also show a rather rapid diversification during the early Spathian (Orchard, 2007; Brayard et al., 2009; Brayard et al., 2019). In addition, the Paris Biota from the earliest Spathian of southeastern Idaho highlights the existence of highly diversified and complex marine ecosystems in the immediate aftermath of the LSC (Brayard et al., 2017). Based on presently known data, the LSC apparently did not have a profound effect on benthic communities. The anoxic settings recorded during the late Smithian reduced considerably above the Smithian/Spathian boundary, potentially due to the cooling event and a renewed oceanic circulation (Lyu et al., 2019; Song H.Y. et al., 2019) and carbonate factory (Galfetti et al., 2008). The recovery after the LSC probably also benefited from the potentially more stable and less deleterious marine environments at the beginning of the Spathian (Zhang et al., 2015). The Spathian interval recorded a profound worldwide reconstruction of marine ecosystems from the tropics to the poles (Song et al., 2020), including the renewed increase in diversity of many clades (Orchard, 2007; Bottjer et al., 2008; Brayard et al., 2009; Song et al., 2011; Hofmann et al., 2013; Chen et al., 2015; Tu et al., 2016; Foster et al., 2017), the occurrence of complex marine ecosystems (Brayard et al., 2017), and potentially the return of more standard marine functional pyramid (Song et al., 2018).

6. CONCLUSIONS

Four ammonoid zones were identified in the three studied sections from the Nanpanjiang Basin, South China. They include the middle Smithian *Flemingites rursiradiatus* and *Owenites koeneni* Zones, and the late Smithian *Anasibirites kingianus* and *Xenoceltites variocostatus* Zones. Our combined analyses show that the late Smithian crisis likely started at the middle/upper Smithian boundary, coinciding with the onset of the positive carbon isotopic excursion. Grain count in thin sections indicates a sudden decrease in richness and abundance in shallow-water settings at the middle/upper Smithian boundary, while deeper water settings show a turnover from bivalve-dominated to ostracod-dominated benthic assemblages. The diversity and abundance of various taxa began to increase again during the early Spathian in shallow-water settings. This was coeval to the rapid resurgence of bivalve-dominated assemblages in deeper basin settings. Overall, these observations

support a rapid regional recovery after the LSC. Size analyses of pyrite framboids and sedimentological field observations support the existence of a relatively short-term disoxic/anoxic event coeval with the LSC, suggesting a potential causal relationship. The known fluctuations of temperatures together with contemporaneous oceanic anoxia and acidification most likely caused the late Smithian crisis.

ACKNOWLEDGEMENTS

We thank Jun Wang, Yiran Cao, Luyi Miao and Yan Feng for their help in the field. This research was supported by the Natural Science Foundation of China (41821001, 41872033), the Strategic Priority Research Program of Chinese Academy of Sciences (XDB26000000), the Research Program the State Key Laboratory of Palaeobiology and Stratigraphy (143106); the French "Investissements d'Avenir" program, project ISITE-BFC (ANR-15-IDEX-03), and the Fundamental Research Funds for National University, China University of Geosciences (Wuhan).

REFERENCES CITED

Bagherpour, B., Bucher, H., Baud, A., Brosse, M., Vennemann, T., Martini, R., and Guodun, K., 2017, Onset, development, and cessation of basal Early Triassic microbialites (BETM) in the Nanpanjiang pull-apart Basin, South China Block: Gondwana Research, v. 44, p. 178–204.

Bailey, T. R., Rosenthal, Y., McArthur, J. M., Van de Schootbrugge, B., and Thirlwall, M. F., 2003, Paleoceanographic changes of the Late Pliensbachian–Early Toarcian interval: a possible link to the genesis of an Oceanic Anoxic Event.: Earth and Planetary Science Letters, v. 212, no. 3–4, p. 307–320.

Bambach, R. K., Knoll, A. H., and Sepkoski, J. J., 2002, Anatomical and ecological constraints on Phanerozoic animal diversity in the marine realm: Proceedings of the National Academy of Sciences, v. 99, no. 10, p. 6854–6859.

Bottjer, D. J., Clapham, M. E., Fraiser, M. L., and Powers, C. M., 2008, Understanding mechanisms for the end-Permian mass extinction and the protracted Early Triassic aftermath and recovery: GSA Today, v. 18, no. 9, p. 4-10.

Brühwiler, T., Brayard, A., Bucher, H., and Guodun, K., 2008, Griesbachian and Dienerian (Early Triassic) Ammonoid Faunas from Northwestern Guangxi and Southern Guizhou (South China): Palaeontology, v. 51, no. 5, p. 1151–1180.

Brühwiler, T., Bucher, H., Brayard, A., and Goudemand, N., 2010a, High-resolution

719 biochronology and diversity dynamics of the Early Triassic ammonoid recovery: The
720 Smithian faunas of the Northern Indian Margin: Palaeogeography Palaeoclimatology
721 Palaeoecology, v. 297, no. 2, p. 491–501.
722 Brühwiler, T., Bucher, H., and Goudemand, N., 2010b, Smithian (Early Triassic) ammonoids
723 from Tulong, South Tibet: Geobios, v. 43, no. 4, p. 403–431.
724 Brühwiler, T., Bucher, H., Goudemand, N., and Galfetti, T., 2012a, Smithian (Early Triassic)
725 ammonoid faunas from Exotic Blocks from Oman: taxonomy and biochronology:
726 Palaeontographica Abteilung A, p. 13–107.
727 Brühwiler, T., Bucher, H., and Krystyn, L., 2012b, Middle and late Smithian (Early Triassic)
728 ammonoids from Spiti, India: Special papers in Palaeontology Series, no. 88, p. 115–
729 174.
730 Brühwiler, T., Bucher, H., Roohi, G., Yaseen, A., and Rehman, K., 2011, A new early
731 Smithian ammonoid fauna from the Salt Range (Pakistan): Swiss Journal of
732 Palaeontology, v. 130, no. 2, p. 187–201.
733 Brühwiler, T., Bucher, H., Ware, D., Hermmann, E., Hochuli, P. A., Roohi, G., Rehman, K.,
734 and Yaseen, A., 2012c, Smithian (Early Triassic) ammonoids from the Salt Range:
735 Special papers in Palaeontology Series, v. 88, p. 1–114.
736 Brühwiler, T., Ware, D., Bucher, H., Krystyn, L., and Goudemand, N., 2010c, New Early
737 Triassic ammonoid faunas from the Dienerian/Smithian boundary beds at the
738 Induan/Olenekian GSSP candidate at Mud (Spiti, Northern India): Journal of Asian
739 Earth Sciences, v. 39, no. 6, p. 724–739.
740 Brayard, A., and Bucher, H., 2008, Smithian (Early Triassic) ammonoid faunas from
741 northwestern Guangxi (South China): taxonomy and biochronology: Fossils and
742 Strata, v. 55, p. 1–184.
743 Brayard, A., Bucher, H., Escarguel, G., Fluteau, F., Bourquin, S., and Galfetti, T., 2006, The
744 Early Triassic ammonoid recovery: Paleoclimatic significance of diversity gradients:
745 Palaeogeography Palaeoclimatology Palaeoecology, v. 239, no. 3–4, p. 374–395.
746 Brayard, A., Bylund, K. G., Jenks, J. F., Stephen, D. A., Olivier, N., Escarguel, G., Fara, E.,
747 and Vennin, E., 2013, Smithian ammonoid faunas from Utah: implications for Early
748 Triassic biostratigraphy, correlation and basinal paleogeography: Swiss Journal of
749 Palaeontology, v. 132, no. 2, p. 141–219.
750 Brayard, A., Escarguel, G., and Bucher, H., 2007, The biogeography of early Triassic
751 ammonoid faunas: Clusters, gradients, and networks: Geobios, v. 40, no. 6, p. 749–
752 765.

753 Brayard, A., Escarguel, G., Bucher, H., Monnet, C., Brühwiler, T., Goudemand, N., Galfetti,
754 T., and Guex, J., 2009, Good genes and good luck: ammonoid diversity and the
755 end-Permian mass extinction: Science, v. 325, no. 5944, p. 1118–1121.
756 Brayard, A., Jenks, J. F., Bylund, K. G., and the Paris Biota team 2019, Ammonoids and
757 nautiloids from the earliest Spathian Paris Biota and other early Spathian localities in
758 southeastern Idaho, USA: Geobios, v. 54, p. 13–36.
759 Brayard, A., Krumenacker, L. J., Botting, J. P., Jenks, J. F., Bylund, K. G., Fara, E., Vennin,
760 E., Olivier, N., Goudemand, N., Saucede, T., Charbonnier, S., Romano, C.,
761 Doguzhaeva, L., Ben, T., Hautmann, M., Stephen, D. A., Thomazo, C., and Escarguel,
762 G., 2017, Unexpected Early Triassic marine ecosystem and the rise of the Modern
763 evolutionary fauna: Science Advances, v. 3, no. 2, p. e1602159.
764 Brosse, M., Brayard, A., Fara, E., and Neige, P., 2013, Ammonoid recovery after the
765 Permian-Triassic mass extinction: a re-exploration of morphological and phylogenetic
766 diversity patterns: Journal of the Geological Society, London, v. 170, p. 225–236.
767 Charbonnier, G., and Follmi, K. B., 2017, Mercury enrichments in lower Aptian sediments
768 support the link between Ontong Java large igneous province activity and oceanic
769 anoxic episode 1a: Geology, v. 45, no. 1, p. 63-66.
770 Chatalov, A., 2013, A Triassic homoclinal ramp from the Western Tethyan realm , Western
771 Balkanides , Bulgaria : Integrated insight with special emphasis on the Anisian outer
772 to inner ramp facies transition: Palaeogeography, Palaeoclimatology, Palaeoecology, v.
773 386, p. 34–58.
774 Chen, J., Tong, J., Song, H., Luo, M., Huang, Y., and Xiang, Y., 2015, Recovery pattern of
775 brachiopods after the Permian–Triassic crisis in South China: Palaeogeography,
776 Palaeoclimatology, Palaeoecology, v. 433, p. 91–105.
777 Chen, Y., Twitchett, R. J., Jiang, H., Richoz, S., Lai, X., Yan, C., Sun, Y., Liu, X., and Wang,
778 L., 2013, Size variation of conodonts during the Smithian–Spathian (Early Triassic)
779 global warming event: Geology, v. 41, no. 8, p. 823–826.
780 Clarkson, M. O., Wood, R. A., Poulton, S. W., Richoz, S., Newton, R. J., Kasemann, S. A.,
781 Bowyer, F., and Krystyn, L., 2016, Dynamic anoxic ferruginous conditions during the
782 end-Permian mass extinction and recovery: Nature Communications, v. 7, p. 12236.
783 Dai, X., Song, H., Brayard, A., and Ware, D., 2019, A new Griesbachian–Dienerian (Induan,
784 Early Triassic) ammonoid fauna from Gujiao, South China: Journal of Paleontology, v.
785 93, no. 1, p. 48–71.
786 Dai, X., and Song, H., 2020, Toward an understanding of cosmopolitanism in deep time: a

case study of ammonoids from the middle Permian to the Middle Triassic: Paleobiology, v. 46, no. 4, p. 533–549.

Enos, P., Jiayong, W., and Lehrmann, D. J., 1998, Death in Guizhou — Late Triassic drowning of the Yangtze carbonate platform: Sedimentary Geology, v. 118, no. 1998, p. 55–76.

Fang, Y., Chen, Z. Q., Kershaw, S., Yang, H., and Luo, M., 2017, Permian–Triassic boundary microbialites at Zuodeng section, Guangxi Province, South China: geobiology and palaeoceanographic implications: Global and planetary change, v. 152, p. 115–128.

Feng, Z., Bao, Z., and Liu, S., 1997, Lithofacies Palaeogeography of Early and Middle Triassic of South China, Beijing, Petroleum Industry Press, 222 p.

Flügel, E., 2010, Microfacies of Carbonate Rocks, Berlin Heidelberg, Springer, 929 p.

Forel, M. B., Crasquin, S., Kershaw, S., and Collin, P. Y., 2013, In the aftermath of the end-P ermian extinction: the microbialite refuge?: Terra Nova, v. 25, no. 2, p. 137–143.

Foster, W. J., Danise, S., Price, G. D., and Twitchett, R. J., 2017, Subsequent biotic crises delayed marine recovery following the late Permian mass extinction event in northern Italy: PloS one, v. 12, no. 3, p. e0172321.

Foster, W. J., Danise, S., Price, G. D., and Twitchett, R. J., 2018, Paleoecological analysis of benthic recovery after the Late Permian mass extinction event in eastern Lombardy, Italy: Palaios, v. 33, no. 6, p. 266–281.

Foster, W. J., Danise, S., Sedlacek, A., Price, G. D., Hips, K., and Twitchett, R. J., 2015, Environmental controls on the post-Permian recovery of benthic, tropical marine ecosystems in western Palaeotethys (Aggtelek Karst, Hungary): Palaeogeography, Palaeoclimatology, Palaeoecology, v. 440, p. 374–394.

Galfetti, T., Bucher, H., Martini, R., Hochuli, P. A., Weissert, H., Crasquin-Soleau, S., Brayard, A., Goudemand, N., Brüehwiler, T., and Guodun, K., 2008, Evolution of Early Triassic outer platform paleoenvironments in the Nanpanjiang Basin (South China) and their significance for the biotic recovery: Sedimentary Geology, v. 204, no. 1–2, p. 36–60.

Galfetti, T., Bucher, H., Ovtcharova, M., Schaltegger, U., Brayard, A., Bruehwiler, T., Goudemand, N., Weissert, H., Hochuli, P. A., Cordey, F., and Guodun, K., 2007a, Timing of the Early Triassic carbon cycle perturbations inferred from new U-Pb ages and ammonoid biochronozones: Earth and Planetary Science Letters, v. 258, no. 3–4, p. 593–604.

Galfetti, T., Hochuli, P. A., Brayard, A., Bucher, H., Weissert, H., and Vigran, J. O., 2007b,

Smithian-Spathian boundary event: Evidence for global climatic change in the wake of the end-Permian biotic crisis: Geology, v. 35, no. 4, p. 291–294.

Gliwa, J., Ghaderi, A., Leda, L., Schobben, M., Tomás, S., Foster, W. J., Forel, M. B., Tabrizi, N. G., Grasby, S. E., Struck, U., Ashouri, A. R., and Korn, D., 2020, Aras Valley (northwest Iran): high-resolution stratigraphy of a continuous central Tethyan Permian–Triassic boundary section: Fossil Record, v. 23, no. 1, p. 33–69.

Goudemand, N., Romano, C., Brayard, A., Hochuli, P. A., and Bucher, H., 2013, Comment on" Lethally hot temperatures during the Early Triassic greenhouse": Science, v. 339, no. 6123, p. 1033–1033.

Goudemand, N., Romano, C., Leu, M., Bucher, H., Trotter, J. A., and Williams, I. S., 2019, Dynamic interplay between climate and marine biodiversity upheavals during the early Triassic Smithian-Spathian biotic crisis: Earth-Science Reviews, v. 195, p. 169–178.

Grasby, S. E., Beauchamp, B., Bond, D. P., Wignall, P. B., and Sanei, H., 2016, Mercury anomalies associated with three extinction events (Capitanian crisis, latest Permian extinction and the Smithian/Spathian extinction) in NW Pangea: Geological magazine, v. 153, no. 2, p. 285–297.

Grasby, S. E., Beauchamp, B., Embry, A., and Sanei, H., 2013a, Recurrent Early Triassic ocean anoxia: Geology, v. 41, no. 2, p. 175–178.

Grasby, S. E., Sanei, H., Beauchamp, B., and Chen, Z. H., 2013b, Mercury deposition through the Permo-Triassic Biotic Crisis: Chemical Geology, v. 351, p. 209-216.

Grasby, S. E., Shen, W., Yin, R., Gleason, J. D., Blum, J. D., Lepak, R. F., Hurley, J. P., and Beauchamp, B., 2017, Isotopic signatures of mercury contamination in latest Permian oceans: Geology, v. 45, no. 1, p. 55–58.

Hammer, Ø., Jones, M. T., Schneebeli-Hermann, E., Hansen, B. B., and Bucher, H., 2019, Are Early Triassic extinction events associated with mercury anomalies? A reassessment of the Smithian/Spathian boundary extinction: Earth-Science Reviews, v. 195, p. 179–190.

Hermann, E., Hochuli, P. A., Mehay, S., Bucher, H., Brühwiler, T., Ware, D., Hautmann, M., Roohi, G., ur-Rehman, K., and Yaseen, A., 2011, Organic matter and palaeoenvironmental signals during the Early Triassic biotic recovery: The Salt Range and Surghar Range records: Sedimentary Geology, v. 234, no. 1–4, p. 19–41.

Hofmann, R., Hautmann, M., Brayard, A., Nüetzel, A., Bylund, K. G., Jenks, J. F., Vennin, E., Olivier, N., and Bucher, H., 2014, Recovery of benthic marine communities from the

855 end-Permian mass extinction at the low latitudes of eastern Panthalassa:
856 Palaeontology, v. 57, no. 3, p. 547–589.
857 Hofmann, R., Hautmann, M., and Bucher, H., 2015, Recovery dynamics of benthic marine
858 communities from the Lower Triassic Werfen Formation, northern Italy: Lethaia, v. 48,
859 no. 4, p. 474–196.
860 Hofmann, R., Hautmann, M., Wasmer, M., and Bucher, H., 2013, Palaeoecology of the
861 Spathian Virgin Formation (Utah, USA) and its implications for the Early Triassic
862 recovery: Acta Palaeontologica Polonica, v. 58, no. 1, p. 149–173.
863 Jattiot, R., Brayard, A., Bucher, H., Vennin, E., Caravaca, G., Jenks, J. F., Bylund, K. G., and
864 Escarguel, G., 2018, Palaeobiogeographical distribution of Smithian (Early Triassic)
865 ammonoid faunas within the western USA basin and its controlling parameters:
866 Palaeontology, v. 61, no. 6, p. 881–904.
867 Jattiot, R., Bucher, H., and Brayard, A., 2020, Smithian (Early Triassic) ammonoid faunas
868 from Exotic Blocks from Timor: taxonomy and biochronology: Palaeontographica
869 Abteilung A, v. 317, no. 1–6, p. 1–137.
870 Jattiot, R., Bucher, H., Brayard, A., Brosse, M., and Jenks, J. F. B., K.G, 2017, Smithian
871 ammonoid faunas from northeastern Nevada: implications for Early Triassic
872 biostratigraphy and correlation within the western USA basin: Palaeontographica
873 Abteilung A, v. 309, p. 1–89.
874 Jattiot, R., Bucher, H., Brayard, A., Monnet, C., Jenks, J. F., and Hautmann, M., 2016,
875 Revision of the genus Anasibirites Mojsisovics (Ammonoidea): an iconic and
876 cosmopolitan taxon of the late Smithian (Early Triassic) extinction: Papers in
877 Palaeontology, v. 2, no. 1, p. 155–188.
878 Jenks, J. F., and Brayard, A., 2018, Smithian (Early Triassic) ammonoids from Crittenden
879 Springs, Elko County, Nevada: taxonomy, biostratigraphy and biogeography: New
880 Mexico Museum of Natural History and Science Bulletin, v. 78, p. 1–175.
881 Jenks, J. F., Monnet, C., Balini, M., Brayard, A., and Meier, M., 2015, Biostratigraphy of
882 Triassic Ammonoids, *in* Klug, C., Kruta, I., Korn, D., Mapes, R. H., and Baets, K. D.,
883 eds., Ammonoid Paleobiology: From macroevolution to paleogeography, Volume 44:
884 Netherlands, Springer, p. 329–388.
885 Kidwell, S. M., 1991, Taphonomic feedback (live/dead interactions) in the genesis of
886 bioclastic beds: keys to reconstructing sedimentary dynamics: Cycles and events in
887 stratigraphy, p. 268–281.
888 Komatsu, T., Takashima, R., Shigeta, Y., Maekawa, T., Tran, H. D., Cong, T. D., Sakata, S.,

Dinh, H. D., and Takahashi, O., 2016, Carbon isotopic excursions and detailed ammonoid and conodont biostratigraphies around Smithian-Spathian boundary in the Bac Thuy Formation, Vietnam: Palaeogeography Palaeoclimatology Palaeoecology, v. 454, p. 65-74.

Lehrmann, D. J., Bentz, J. M., Wood, T., Goers, A., Dhillon, R., Akin, S., Li, X. W., Payne, J. L., Kelley, B. M., Meyer, K. M., Schaal, E. K., Suarez, M. B., Yu, M. Y., Qin, Y. J., Li, R. X., Minzoni, M., and Henderson, C. M., 2015, Environmental controls on the genesis of maeine microbialites and dissolution surface associated with the end-Permian mass extinction: new sections and observations from the Nanpanjiang Basin, South China: Palaios, v. 30, no. 7, p. 529–552.

Leu, M., Bucher, H., and Goudemand, N., 2019, Clade-dependent size response of conodonts to environmental changes during the late Smithian extinction: Earth-Science Reviews, v. 195, no. 52–67.

Li, M., Song, H., Woods, A. D., Dai, X., and Wignall, P. B., 2019, Facies and evolution of the carbonate factory during the Permian–Triassic crisis in South Tibet, China: Sedimentology, v. 59, p. 646–678.

Liu, X., and Song, H., 2020, Automatic identification of fossils and abiotic grains during carbonate microfacies analysis using deep convolutional neural networks: Sedimentary Geology, v. 410, p. 105790.

Lyu, Z. Y., Zhang, L., Algeo, T. J., Zhao, L. S., Chen, Z. Q., Li, C., Ma, B. A., and Ye, F. H., 2019, Global-ocean circulation changes during the Smithian-Spathian transition inferred from carbon-sulfur cycle records: Earth-Science Reviews, v. 195, p. 114–132.

Mathes, G. H., van Dijk, J., Kiessling, W., and Steinbauer, M. J., 2021, Extinction risk controlled by interaction of long-term and short-term climate change: Nature Ecology & Evolution. doi:10.1038/s41559-020-01377-w.

Mu, L., Zakharov, Y., Li, W.-Z., and Shen, S.-Z., 2007, Early Induan (Early Triassic) cephalopods from the Daye Formation at Guiding, Guizhou Province, South China: Journal Information, v. 81, no. 5, p. 858–872.

Orchard, M. J., 2007, Conodont diversity and evolution through the latest Permian and Early Triassic upheavals: Palaeogeography, Palaeoclimatology, Palaeoecology, v. 252, no. 1–2, p. 93–117.

Pérez-López, A., and Pérez-Valera, F., 2012, Tempestite facies models for the epicontinental Triassic carbonates of the Betic Cordillera (southern Spain): Sedimentology, v. 59, p. 646–678.

Payne, J. L., Lehrmann, D. J., Wei, J., Orchard, M. J., Schrag, D. P., and Knoll, A. H., 2004, Large perturbations of the carbon cycle during recovery from the end-Permian extinction: Science, v. 305, no. 5683, p. 506–509.

Romano, C., Goudemand, N., Vennemann, T. W., Ware, D., Schneebeli-Hermann, E., Hochuli, P. A., Bruehwiler, T., Brinkmann, W., and Bucher, H., 2013, Climatic and biotic upheavals following the end-Permian mass extinction: Nature Geoscience, v. 6, no. 1, p. 57–60.

Scheyer, T. M., Romano, C., Jenks, J., and Bucher, H., 2014, Early Triassic marine biotic recovery: the predators' perspective: PLoS One, v. 9, no. 3, p. e88987.

Scotese, C. R., 2014, Atlas of Middle & Late Permian and Triassic Paleogeographic maps, maps 43–48 from volume 3 of the PALEOMAP Atlas for ArcGIS (Jurassic and Triassic) and maps 49–52 from volume 4 of the PALEOMAP PaleoAtlas for ArcGIS (Late Paleozoic): Mollweide Projection, PALEOMAP Project, Evanston, IL.

Shigeta, Y., Komatsu, T., Maekawa, T., and Tran, H. D., 2014, Olenekian (Early Triassic) stratigraphy and fossil assemblages in northeastern Vietnam: National Museum of Nature and Science, v. 45, p. 1–309.

Shigeta, Y., Zakharov, Y. D., Maeda, H., and Popov, A. M., 2009, The Lower Triassic System in the Abrek Bay Area, South Primorye, Russia, Tokyo, National Museum of Nature and Science, 218 p.

Song, H., Tong, J., Algeo, T. J., Horacek, M., Qiu, H., Song, H., Tian, L., and Chen, Z.-Q., 2013, Large vertical δ 13 C DIC gradients in Early Triassic seas of the South China craton: implications for oceanographic changes related to Siberian Traps volcanism: Global and Planetary Change, v. 105, p. 7–20.

Song, H., Huang, S., Jia, E., Dai, X., Wignall, P. B., and Dunhill, A. M., 2020, Flat latitudinal diversity gradient caused by the Permian–Triassic mass extinction: Proceedings of the National Academy of Sciences, v. 117, no. 30, p. 17578-17583.

Song, H., Song, H., Tong, J., Gordon, W. G., Wignall, B. P., Tian, L., Zheng, W., Algeo, J. T., Liang, L., Bai, R., Wu, K., and Ariel, A. D., 2021, Conodont calcium isotopic evidence for multiple shelf acidification events during the Early Triassic: Chemical Geology, v. 562, p. 120038.

Song, H., Wignall, P. B., Chen, Z. Q., Tong, J., Bond, D. P. G., Lai, X., Zhao, X., Jiang, H., Yan, C., Niu, Z., Chen, J., Yang, H., and Wang, Y., 2011, Recovery tempo and pattern of marine ecosystems after the end-Permian mass extinction: Geology, v. 39, no. 8, p. 739–742.

Song, H., Wignall, P. B., Chu, D., Tong, J., Sun, Y., Song, H., He, W., and Tian, L., 2014, Anoxia/high temperature double whammy during the Permian-Triassic marine crisis and its aftermath: Scientific Reports, v. 4.

Song, H., Wignall, P. B., and Dunhill, A. M., 2018, Decoupled taxonomic and ecological recoveries from the Permo-Triassic extinction: Science Advances, v. 4, no. 10, p. eaat5091.

Song, H., Wignall, P. B., Tong, J., Bond, D. P., Song, H., Lai, X., Zhang, K., Wang, H., and Chen, Y., 2012, Geochemical evidence from bio-apatite for multiple oceanic anoxic events during Permian–Triassic transition and the link with end-Permian extinction and recovery: Earth and Planetary Science Letters, v. 353, p. 12–21.

Song, H., Wignall, P. B., and Dunhill, A. M., 2018, Decoupled taxonomic and ecological recoveries from the Permo-Triassic extinction: Science Advances, v. 4, no. 10, p. eaat5091.

Song, H. Y., Du, Y., Algeo, T. J., Tong, J. N., Owens, J. D., Song, H. J., Tian, L., Qiu, H., Zhu, Y., and Lyons, T. W., 2019, Cooling-driven oceanic anoxia across the Smithian/Spathian boundary (mid-early Triassic): Earth-Science Reviews, v. 195, p. 133–146.

Stanley, S. M., 2009, Evidence from ammonoids and conodonts for multiple Early Triassic mass extinctions: Proceedings of the National Academy of Sciences of the United States of America, v. 106, no. 36, p. 15264–15267.

Sun, Y., Joachimski, M. M., Wignall, P. B., Yan, C., Chen, Y., Jiang, H., Wang, L., and Lai, X., 2012, Lethally Hot Temperatures During the Early Triassic Greenhouse: Science, v. 338, no. 6105, p. 366–370.

Sun, Y. D., Wignall, P. B., Joachimski, M. M., Bond, D. P. G., Grasby, S. E., Sun, S., Yan, C. B., Wang, L. N., Chen, Y. L., and Lai, X. L., 2015, High amplitude redox changes in the late Early Triassic of South China and the Smithian–Spathian extinction: Palaeogeography, Palaeoclimatology, Palaeoecology, v. 427, p. 62–78.

Thibodeau, A. M., Ritterbush, K., Yager, J. A., West, A. J., Ibarra, Y., Bottjer, D. J., Berelson, W. M., Bergquist, B. A., and Corsetti, F. A., 2016, Mercury anomalies and the timing of biotic recovery following the end-Triassic mass extinction: Nature Communications, v. 7. p. 11147.

Tong, J., Chu, D., Liang, L., Shu, W., Song, H., Song, T., Song, H., and Wu, Y., 2018, Triassic integrative stratigraphy and timescale of China: Science China Earth Sciences, v. 62, no. 1, p. 189–222.

991 Tong, J., Zuo, J., and Chen, Z. Q., 2007, Early Triassic carbon isotope excursions from South
992 China: Proxies for devastation and restoration of marine ecosystems following the
993 end-Permian mass extinction: Geological Journal, v. 42, no. 3–4, p. 371–389.
994 Tozer, E. T., 1965, Lower Triassic stages and Ammonoid zones of Arctic Canada: Paper of
995 the Geological Survey of Canada, v. 65-12, p. 1–14.
996 Tozer, E. T., 1981, Triassic Ammonoidea: geographic and stratigraphic distribution, *in* House,
997 M. R., and Senior, J. R., eds., The ammonoidea: the evolution, classification, mode of
998 life and geological usefulness of a major fossil group: London, The Systematics
999 Association, p. 397–431.
1000 Tu, C. Y., Chen, Z. Q., and Harper, D. A. T., 2016, Permian-Triassic evolution of the Bivalvia:
1001 Extinction-recovery patterns linked to ecologic and taxonomic selectivity:
1002 Palaeogeography Palaeoclimatology Palaeoecology, v. 459, p. 53–62.
1003 Wan, J., Yuan, A., Crasquin, S., Jiang, H., Yang, H., and Hu, X., 2019, High-resolution
1004 variation in ostracod assemblages from microbialites near the Permian-Triassic
1005 boundary at Zuodeng, Guangxi region, South China: Palaeogeography,
1006 Palaeoclimatology, Palaeoecology, v. 535, p. 109349.Wang, X. D., Cawood, P. A.,
1007 Zhao, H., Zhao, L. S., Grasby, S. E., Chen, Z. Q., Wignall, P. B., Lv, Z. Y., and Han,
1008 C., 2018, Mercury anomalies across the end Permian mass extinction in South China
1009 from shallow and deep water depositional environments: Earth and Planetary Science
1010 Letters, v. 496, p. 159–167.
1011 Wang, X. D., Cawood, P. A., Zhao, H., Zhao, L. S., Grasby, S. E., Chen, Z. Q., and Zhang, L.,
1012 2019, Global mercury cycle during the end-Permian mass extinction and subsequent
1013 Early Triassic recovery: Earth and Planetary Science Letters, v. 513, p. 144–155.
1014 Widmann, P., Bucher, H., Leu, M., Vennemann, T., Bagherpour, B., Schneebeli-Hermann, E.,
1015 Goudemand, N., and Schaltegger, U., 2020, Dynamics of the Largest Carbon Isotope
1016 Excursion During the Early Triassic Biotic Recovery: Frontiers in Earth Science, v. 8,
1017 no. 196.
1018 Wignall, P. B., and Twitchett, R. J., 1996, Oceanic anoxia and the end Permian mass
1019 extinction: Science, v. 272, no. 5265, p. 1155–1158.
1020 Wu, K., Tian, L., Liang, L., Metcalfe, I., Chu, D., and Tong, J., 2019, Recurrent biotic
1021 rebounds during the Early Triassic: biostratigraphy and temporal size variation of
1022 conodonts from the Nanpanjiang Basin, South China: Journal of the Geological
1023 Society, v. 176, no. 6, p. 1232–1246.
1024 Yang, Z., Yin, H., Wu, S., Yang, F., Ding, M., and Xu, G., 1987, Permian-Triassic boundary

stratigraphy and faunas of South China, Beijing, Geological Publishing House, 379 p.:
Zhang, F., Algeo, T. J., Cui, Y., Shen, J., Song, H., Sano, H., Rowe, H., and Anbar, A. D., 2019a, Global-ocean redox variations across the Smithian-Spathian boundary linked to concurrent climatic and biotic changes: Earth-Science Reviews, v. 195, p. 147–168.
Zhang, F., Romaniello, S. J., Algeo, T. J., Lau, K. V., Clapham, M. E., Richoz, S., Herrmann, A. D., Smith, H., Horacek, M., and Anbar, A. D., 2018, Multiple episodes of extensive marine anoxia linked to global warming and continental weathering following the latest Permian mass extinction: Science Advances, v. 4, no. 4, p. e1602921.
Zhang, L., Orchard, M. J., Brayard, A., Algeo, T. J., Zhao, L., Chen, Z.-Q., and Zhengyi, L., 2019b, The Smithian/Spathian boundary (late Early Triassic): A review of ammonoid, conodont, and carbon-isotopic criteria: Earth-Science Reviews, v. 195, p. 7–36.